

Are There Any Counteracting Effects that Reduce the Global
Warming Benefits Attributed to Black Carbon Controls?
Assessment of Cloud Drop Number Concentration Changes
and its Importance in Modeling Cloud Albedo Effects on
Climate

Report to the
California Air Resources Board
Contract 09-337

Prepared by:

Dr. Lynn M. Russell and Dr. Ranjit Bahadur

Scripps Institution of Oceanography
University of California at San Diego
9500 Gilman Drive, La Jolla CA 92093-0221

December 2012

DISCLAIMER

This report was prepared by the University of California, San Diego (Contractor) as an account of work sponsored by the California Air Resources Board (CARB), under contract # 09-337. The statements and conclusions in this report are those of the contractor, and not necessarily of CARB. The mention of any commercial products, their use in conjunction with material reported here, or their source is not to be construed as an actual or implied endorsement of such products.

ACKNOWLEDGEMENTS

We thank Dr. Nehzat Motallebi for project management support and guidance. We thank Dr. V. Ramanathan for guidance and insight on radiative forcing by black carbon and Dr. Kim Prather (UCSD) for providing size and chemistry resolved field measurements of aerosols in California.

We gratefully acknowledge Dr. Mark Jacobson (Stanford) and Dr. John Seinfeld (Caltech) for acting as project consultants, and for providing global climate model calculations as comparative data sets.

Dr. Peter Adams (Carnegie Mellon) and Dr. Athanasios Nenes (Georgia Tech) provided additional guidance and cloud parameterizations.

The work described in this report was primarily accomplished by UCSD Staff Research Associate Dr. Ranjit Bahadur and Scripps Faculty Dr. Lynn M. Russell.

This Report was submitted in fulfillment of ARB contract number 09-337 by Scripps Institution of Oceanography, University of California at San Diego under the sponsorship of the California Air Resources Board. Work was completed as of August 2012.

TABLE OF CONTENTS

List of Tables	v
List of Figures	vii
List of Acronyms	ix
Abstract	1
Executive Summary	3
1.0 Introduction	10
1.1 Motivation	
1.2 Prior Work	
1.3 Research Objectives	
1.4 Structure of Report	
2.0 California Aerosol Case Studies (Task 1)	13
2.1 Introduction	
2.2 Representative Case Studies	
2.3 External Mixing State of Aerosol	
2.4 Aerosol Size Distribution	
2.5 Internal Mixing State of Aerosol	
2.6 Conclusions	
3.0 Microphysics Aerosol-Cloud Modeling (Task 2)	22
3.1 Introduction	
3.2 Aerosol-Cloud Parcel Model	
3.3 Inclusion of Nitrate Equilibrium	
3.4 Incorporation of Calculated Updraft	
3.5 Modeling Meteorological Conditions	
3.6 Conclusions	
4.0 Analysis of Model Scenarios (Task 2)	31
4.1 Introduction	
4.2 Baseline Simulations	
4.3 Identification of Activated Droplets	
4.4 BC Mitigation Scenarios	
4.5 Observed Trends	
4.6 Conclusions	
5.0 Comparison to GCM Results (Task 3)	43
5.1 Introduction	
5.2 GISS-TOMAS results	
5.3 GATOR-GCCM results	

5.4	California Domain Simulations	
5.5	Validation with Surface Measurements	
5.6	Comparison of Baseline Calculations	
5.7	Comparison of Mitigation Experiments	
5.8	Conclusions	
6.0	Sensitivity Studies (Task 4)	55
6.1	Introduction	
6.2	Impact of Model Mechanisms	
6.3	Impact of Internal Mixing State	
6.4	Impact of Updraft Rate	
6.5	Comparison with GCM Parameterization	
7.0	Conclusions and Findings	62
7.1	Primary Conclusions	
7.2	Research Highlights	
	References	65

LIST OF TABLES

Table 0.1: The number concentration of the total aerosol particles (N_a), black carbon particles (N_b), cloud droplets (N_c), black carbon cloud droplets (N_{bc}), average cloud droplet diameter (D_c) are summarized for the California case studies in this work.

Table 2.1: Selected sampling sites and dates for field measurements in this study.

Table 2.2: Total number of aerosol particle types resolved by external mixing state measured using ATOFMS and particle sizing equipment.

Table 2.3: Measured aerosol particle and constituent component densities used to determine internal mixing state.

Table 2.4: Average fraction and possible range of compositions for the internal mixing state of the aerosol particle types using five constituent species measured in this study.

Table 4.1: The number concentration of the total aerosol particles (N_a), black carbon particles (N_b), cloud droplets (N_c), black carbon cloud droplets (N_{bc}), average cloud droplet diameter (D_c), maximum supersaturation (S_{max}), and corresponding updraft velocity (U) for the five baseline case studies.

Table 4.2: The number concentration of the total aerosol particles (N_a), black carbon particles (N_b), cloud droplets (N_c), black carbon cloud droplets (N_{bc}), change in total aerosol mass (m), average cloud droplet diameter (D_c), maximum supersaturation (S_{max}), and corresponding updraft velocity (U) for the 50% and 90% BC Mitigation Scenarios.

Table 4.3: Total number of activated cloud drops and fraction of total particles activated resolved by particle type for the baseline case studies.

Table 5.1: List of collocated IMPROVE network sites used for validating aerosol mass measurements from GCM calculations and observations used in this study.

Table 5.2: Monthly mean mass concentrations of PM_{2.5} from the IMPROVE network and GCM calculations used in this study.

Table 5.3: Comparison of the total aerosol and cloud droplet number concentration for the baseline case studies at the five California field sites from observations (this study) and from the *Jacobson [2010]* and *Chen et al. [2010a]* models.

Table 5.4: Percent change in the total aerosol and cloud droplet number concentrations for the field studies under the 50% BC and 90% BC (this work), as well as NFS (*Jacobson* [2010]) and HC (*Chen et al.* [2010a]) mitigation scenarios. The North Hemisphere average is used for the Jacobson model.

Table 6.1: Average change in number of activated cloud droplets when aerosol particle types are treated as being internally mixed and as pure components.

Table 6.2: Comparison of cloud droplet number concentration and maximum supersaturation for the case studies obtained using the aerosol-cloud parcel model and the Nenes parameterization.

LIST OF FIGURES

Figure 0.1: Uncertainty in total TOA forcing attributed to BC from various GCM simulations as a function of global BC burden (from Chung and Seinfeld [2002]).

Figure 2.1: Field campaigns with available ATOFMS aerosol measurements chosen to represent different ambient conditions in California.

Figure 2.2: Distributions of the Sulfate, Nitrate, OC and BC particle types determined at the field sites included in this study. The first column illustrates normalized fractions from the ATOFMS, the second column illustrates number size distributions from the sizing instruments, and the third column illustrates the corresponding mass size distribution. Measurements are from Trinidad Head, Riverside, Long Beach, La Jolla, and Sacramento.

Figure 2.3: Internal mixing state of the (a) BC Particle type, (b) OC Particle type, (c) Sulfate Particle type, and (d) Nitrate Particle types used in this study. The mass fractions of the pure components are illustrated as BC (grey), OC (green), Ammonium Sulfate (red), Ammonium Nitrate (blue), and Sodium Chloride (yellow).

Figure 3.1: Aerosol-Cloud interaction processes included in the parcel model.

Figure 3.2: Hygroscopic growth curves for Ammonium Sulfate particles in a Sulfate-Nitrate mixture determined from the aerosol parcel model.

Figure 3.3: Hygroscopic growth curves for Ammonium Nitrate in a sulfate-nitrate mixture determined from the aerosol parcel model.

Figure 3.4: Temperature and RH profiles of the model stratocumulus cloud used in this study to represent common California conditions.

Figure 4.1: Parcel model simulations of the (a) Altitude, (b) RH, (c) liquid water content, and (d) updraft velocity for baseline simulations over a single cloud cycle.

Figure 4.2: Parcel model simulations of the BC particle size distribution from (a) TH, (b) SA, (c) LB, (d) LJ, and (e) RV cases. Dotted lines are below cloud ($t=50$ s), dashed lines are in-cloud before max RH ($t=150$ s), and solid lines are in-cloud after max RH ($t=250$ s).

Figure 4.3: Parcel model simulations of the (a-e) cloud droplet number concentration and (f-j) fraction of particles activated for externally mixed particle populations corresponding a single cloud processing cycle. The base and 50% BC mitigation cases are illustrated.

Figure 5.1: Representative CDN and aerosol size distributions from the nested California GCM year-long simulation performed as a part of this work.

Figure 5.2: Monthly averages for the total PM_{2.5} mass concentration of EC, OC, Sulfate, and Nitrate from filter based measurements from nearly collocated IMPROVE network sites, as well as from *Jacobson* [2010] and *Chen et al.* [2010a] climate models, and monthly averages based on ATOFMS and particle size measurements used for initializing the parcel model.

Figure 5.3: Comparison of the number size distributions of the total particles, BC type particles, and Cloud droplets.

Figure 5.4: Comparison of Total aerosol particle concentration and CDN totals between the *Jacobson* [2010] and *Chen et al.* [2010a] models compared to the field observations used to initialize the parcel model.

Figure 6.1. Comparison of the (a) total CDN and (b) CDN/Particle ratio determined from the GCMs using a full climate simulation, and by applying the parcel model and meteorology described in this work to the aerosol concentrations determined from the GCMs.

Figure 6.2. The total number of particles activated for (a) Sulfate, (b) Nitrate, (c) OC, and (d) EC type particles when no internal mixing is allowed, compared to the internal mixing states described in Chapter 2.

Figure 6.3: Parcel model simulations of the dependence on the updraft velocity operating in fixed updraft and energy conservation mode: (a) maximum supersaturation and (b) cloud droplet number concentration.

Figure 6.4. Comparison of the (a) total CDN and (b) CDN/Particle ratio determined from the GCMs using a full climate simulation, and by applying the parcel model and meteorology described in this work to the aerosol concentrations determined from the GCMs.

LIST OF ACRONYMS

BC	Black Carbon
EC	Elemental Carbon
OC	Organic Carbon
ATOFMS	Aerosol Time of Flight Mass Spectrometry
FTIR	Fourier Transform Infrared
AMS	Aerosol Mass Spectrometry
GCM	General Circulation Model
CDN	Cloud Droplet Number
CCN	Cloud Condensation Nuclei
TH	Trinidad Head field site
RV	Riverside field site
LB	Long Beach field site
LJ	La Jolla field site
SA	Sacramento aircraft measurements
HGF	Hygroscopic Growth Factor
TOA	Top of Atmosphere

ABSTRACT

This report provides an assessment of the relative importance of the first indirect aerosol effect of black carbon forcing for California's climate constrained with measurements by developing a balanced approach between observations, data analyses, and modeling studies. Previous studies in California have indicated that emission control policies have resulted in a 50% decline in BC aerosols. This decline is expected to have a cooling effect due to reduced direct absorption, but the impact on cloud processes is less certain. The report will also address the importance of the internal mixing state and hygroscopicity of the aerosols in addition to total concentration on the secondary aerosol effects.

The study consisted of four primary components: (i) analysis of available measurements and construction of BC case studies constrained by field measurements, (ii) determination of aerosol impact on warm cloud droplet numbers using a sectional parcel model, (iii) downscaling scenarios with reduced BC concentrations compared to observations, and (iv) comparison with global climate models. We identified five field campaigns in California that represent a variety of ambient conditions: clean and polluted marine, polluted urban, and biomass burning dominated. Using co-located ATOFMS measurements of chemical tracers and APS/SMPS number size distributions we described the physical (size and mass) and chemical (both internal and external mixing states) properties of the aerosol. We used our detailed parcel model in conjunction with measured cloud profiles to analyze the evolution of aerosol number size distributions, and determined the total number of activated cloud droplets based on the growth of a mode at 10 micrometers. We repeated the model analysis using scenarios constraining the BC dominated particle types by 50% and 90% to estimate the impact of BC mitigation on cloud droplet population, and compared the local results roughly with those predicted from two GCMs for base (total emissions) and BC mitigated cases. Finally, we also completed a number of sensitivity studies to describe a variety of observed ambient conditions by altering the updraft velocity, allowing for adiabatic cooling, changing the air entrainment rate, and conserving the total available water vapor.

In California, we find that BC-type particles contributed between 16 and 20% of cloud droplets even in the presence of more hygroscopic particles. Reducing BC particle concentration by 50% decreased the cloud droplet concentration by between 6% and 9% resulting in the formation of fewer, larger cloud droplets that correspond to a lower cloud albedo. This trend qualitatively agrees with the GCM calculations of *Chen et al.* [2010a] when climate feedbacks are excluded and with *Jacobson* [2010] only when the BC is treated as being hydrophilic. The implications of this comparison are that in addition to total number concentration, the internal mixing state of the BC is also a significant factor in determining the net impact on clouds. For regions like California, where BC mitigation targets primarily fossil fuel sources, the cloud albedo effect of BC particles may partially offset the climate benefits of direct forcing reduction. The study does not consider

the cloud burning effects of BC, since it is beyond the scope of this project. As studies have shown, the cloud-burning effects of BC can enhance the climate benefits of direct forcing reduction.

EXECUTIVE SUMMARY

Background: Black carbon (BC), the main light-absorbing component of soot is the principal absorber of visible solar radiation in the atmosphere. *Ramanathan and Carmichael* [2008] estimated that BC is the second largest contributor to global warming with a radiative forcing of 0.9 W/m^2 , compared to 1.6 W/m^2 for CO_2 [*Forster et al.*, 2007]. Atmospheric BC also reduces regional rainfall and changes the spatial distribution of precipitation [*Chung et al.*, 2005; *Menon et al.*, 2002], further impacting regional climate. BC aerosol particles have an atmospheric lifetime of the order of one week [*Ogren and Charlson*, 1983; *Stier et al.*, 2007] and are not well mixed in the atmosphere but are instead geographically and temporally correlated to emission sources. Reducing BC emissions therefore has been proposed as a control strategy to offset short-term climate changes [*Jacobson*, 2002]. Aggressive control policies for diesel emissions in California have produced a near 50% decrease in BC concentrations (while non-absorbing particles have remained nearly constant), resulting in an estimated change in the direct radiative forcing of -1.4 W m^{-2} over the State [*Bahadur et al.*, 2011].

BC particles also impact the climate in a series of feedbacks through their interaction with clouds and temperature [*Jacobson*, 2002; *Koch and Del Genio*, 2010]. BC particles internally mixed with or coated by hygroscopic species serve as efficient cloud condensation nuclei (CCN) for both warm and mixed-phase clouds [*Andreae and Rosenfeld*, 2008; *Dusek et al.*, 2006; *Koehler et al.*, 2009; *Lammel and Novakov*, 1995]. Perturbations to the BC concentration can therefore change the cloud droplet number (CDN) concentration and droplet size [*Roberts et al.*, 2003b], which in turn influence both the cloud optical properties and cloud lifetime. These two so-called aerosol indirect effects are thought to have a net cooling effect on the atmosphere [*Lohmann and Feichter*, 2005]. Competing semi-direct effects are found to decrease the cloud cover by stabilizing the atmosphere through warming [*Hansen et al.*, 1997] and to increase absorption by the cloud, helping to burn it off [*Jacobson*, 2006; *Ten Hoeve et al.*, 2012]. In contrast to the direct aerosol effect, the net climate forcing due to these cloud feedbacks and semi-direct effects is highly uncertain [*Forster et al.*, 2007] and may be either a significant offset, or addition, to the direct effect (Figure 1). An assessment of the degree to which the indirect effects of reducing BC offset or enhance the direct effects is needed to quantify the overall mitigation of climate change by BC on which policies can be constructed.

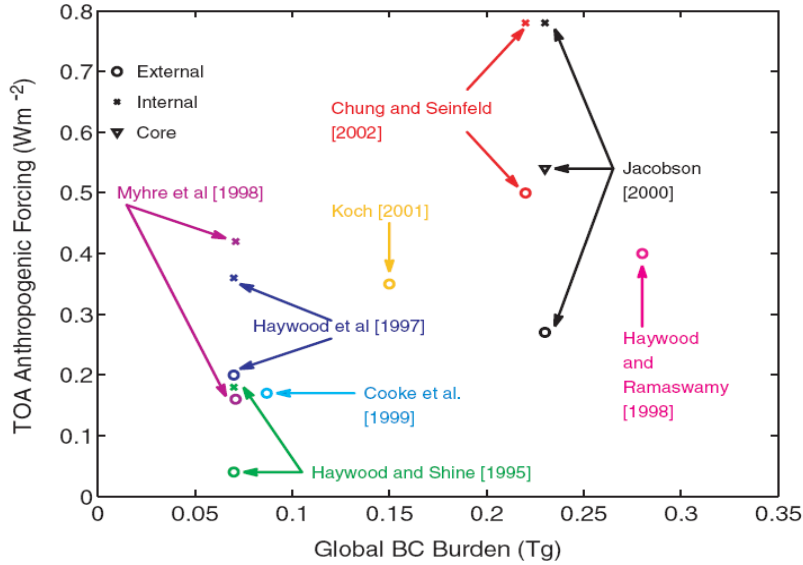


Figure 0.1: Uncertainty in total TOA forcing attributed to BC from various GCM simulations as a function of global BC burden (from Chung and Seinfeld [2002]).

Methods: General circulation models (GCMs) with explicit aerosol-cloud interactions are the principal tools for investigating the indirect effects of BC on CDN concentrations. A recent multi-model comparison [Koch et al., 2011] concluded that soot removal could either increase or decrease the cloud droplet number with the final response depending on a combination of factors including the composition and size of the soot particles, the magnitude of soot change caused by emissions reduction, as well as the non-linear response of the indirect effect itself. In this work, we focus only on the change in CDN concentration from reducing BC particles and can evaluate one part of the climate benefit of a BC reduction.

To assess the differences in cloud parameterizations and the representation of aerosol composition, size, and concentration within different GCM models, we employ a parcel model that connects detailed cloud chemistry and microphysics with a calculated supersaturation profile [Guibert et al., 2003; Snider et al., 2003]. Since the parcel model does not include the feedback of BC on the temperature profile, the semi-direct effects are not assessed in this study. Here, we use the Russell and Seinfeld [1998] parcel model initialized with cloud and aerosol measurements from field studies in California. The model predicts the growth of aerosol populations for explicit external and internal mixtures of aerosol species, accounting for coagulation, condensation, deposition, activation, and nucleation. For non-water components, both particle number and mass are conserved as particles grow. Maximum super-saturation, activated drop size, and number of droplets formed due to water condensation are determined kinetically. Aerosol particles are described as internal mixtures of six species (water, black carbon, organic carbon, ammonium sulfate, ammonium nitrate, and sodium chloride) and are allowed to be in external mixtures of different particle types.

The impact of reducing BC is determined by repeating our model simulations for 50% and 90% reduction in BC compared with the base (measured) case, the results of which are also compared with GCM results from *Chen et al.* [2010a] and *Jacobson* [2010]. These comparisons allow us to address the following questions: (1) Does BC contribute significantly to cloud droplets in representative aerosol populations? (2) How do the aerosol and cloud number size distributions determined in GCMs compare with results from a detailed parcel model? (3) How does BC mitigation impact the total cloud droplet concentration?

Cloud Droplet Results: The number concentration of aerosol particles, the number concentration of cloud droplets, and the mean cloud droplet diameter are summarized in Table 0.1 for five observationally constrained baseline cases in California, with corresponding 50% BC mitigation scenarios. Although the sites represent different dominant emission scenarios (resulting in differences in aerosol size, concentration, and chemical composition), we observe several consistent trends. First, the number concentration of cloud droplets (ranging between 160 cm^{-3} at Trinidad Head, a clean marine environment, and 301 cm^{-3} at Riverside, a polluted urban environment) is directly correlated to the ambient number concentration of aerosol particles (7287 cm^{-3} at Trinidad Head and 14321 cm^{-3} at Riverside), while the average droplet diameter is inversely related.

Since BC-dominated particle type typically comprise between 20% and 30% by number of the total particles at all sites, the 50% BC mitigation scenario results in a reduction between 7% (at Trinidad Head) and 11% (at Long Beach) the total particle number concentration. The decrease in particle number concentration of cloud drops however is only between 5% (at Trinidad Head and Riverside) and 9% (at Long Beach), which is disproportionately smaller than the reduction in particle concentration. We consider the major implication of the discrepancy to be that in addition to the total size distribution, the differences in aerosol chemical composition between the Trinidad Head and Long Beach cases are also a contributing factor to the differences in activation of cloud droplets. The “rebound” effect in cloud droplet concentration is observed because the decrease in activated BC droplets is balanced to a certain extent by an increase in the number concentration of activated particles from the comparatively more hygroscopic Sulfate and Nitrate rich particles.

The implications for regional climate are that if only BC-rich particles are reduced (in polluted environments), the many CCN that do not contain BC still activate in place of the BC aerosol particles preserving the cloud droplet populations and mean diameters. Even though the decrease in CDN is much less than proportional to the BC reduction (due to an associated increase in the number of activated non-BC particles), the net effect of BC reduction is a small decrease in the total CDN concentration.

Location	N_a cm^{-3}	N_b cm^{-3}	N_c cm^{-3}	N_{bc} cm^{-3}	D_c μm
Base Case (measurements)					
Trinidad Head	7287	1015	160	31	9.8
Riverside	14321	2130	301	59	8.6
La Jolla	10178	2112	216	64	9.3
Long Beach	11295	2656	289	111	8.7
Sacramento	9231	1686	221	77	9.0
50% BC Mitigation Case					
Trinidad Head	6780	508	151	17	10.2
Riverside	13286	1065	284	28	9.8
La Jolla	9122	1056	202	31	9.6
Long Beach	9987	1328	216	55	8.7
Sacramento	8388	843	178	38	9.1

Table 0.1: The number concentration of the total aerosol particles (N_a), black carbon particles (N_b), cloud droplets (N_c), black carbon cloud droplets (N_{bc}), average cloud droplet diameter (D_c) are summarized for the California case studies in this work.

Comparison with GCMs: Since the parcel model used in this study constrains only the first aerosol indirect effect, we get a better understanding of the climate implications by comparing the mitigation scenario with those from general circulation models. In this work, the BC mitigation scenarios represented by the half-fossil (HF) fuel BC case from *Chen et al.* [2010a] and the no fossil soot (NFS) case from *Jacobson* [2010] are used. We find a direct correlation in the number concentrations for both total aerosol particles and total CDN concentrations represented in the three models, i.e. all three models predict a higher concentration in the more polluted cases. Relative to this study, both GCMs have a larger absolute concentration for both total aerosol and cloud droplets. The change in CDN concentration for BC mitigation scenarios follow the reductions in BC aerosol concentration, with the *Chen et al.* [2010a] model (showing the largest reduction) and the [*Jacobson, 2010*] model (finding the smallest magnitude change) bracketing calculations from the parcel model reported here. These trends are illustrated in Figure 0.2.

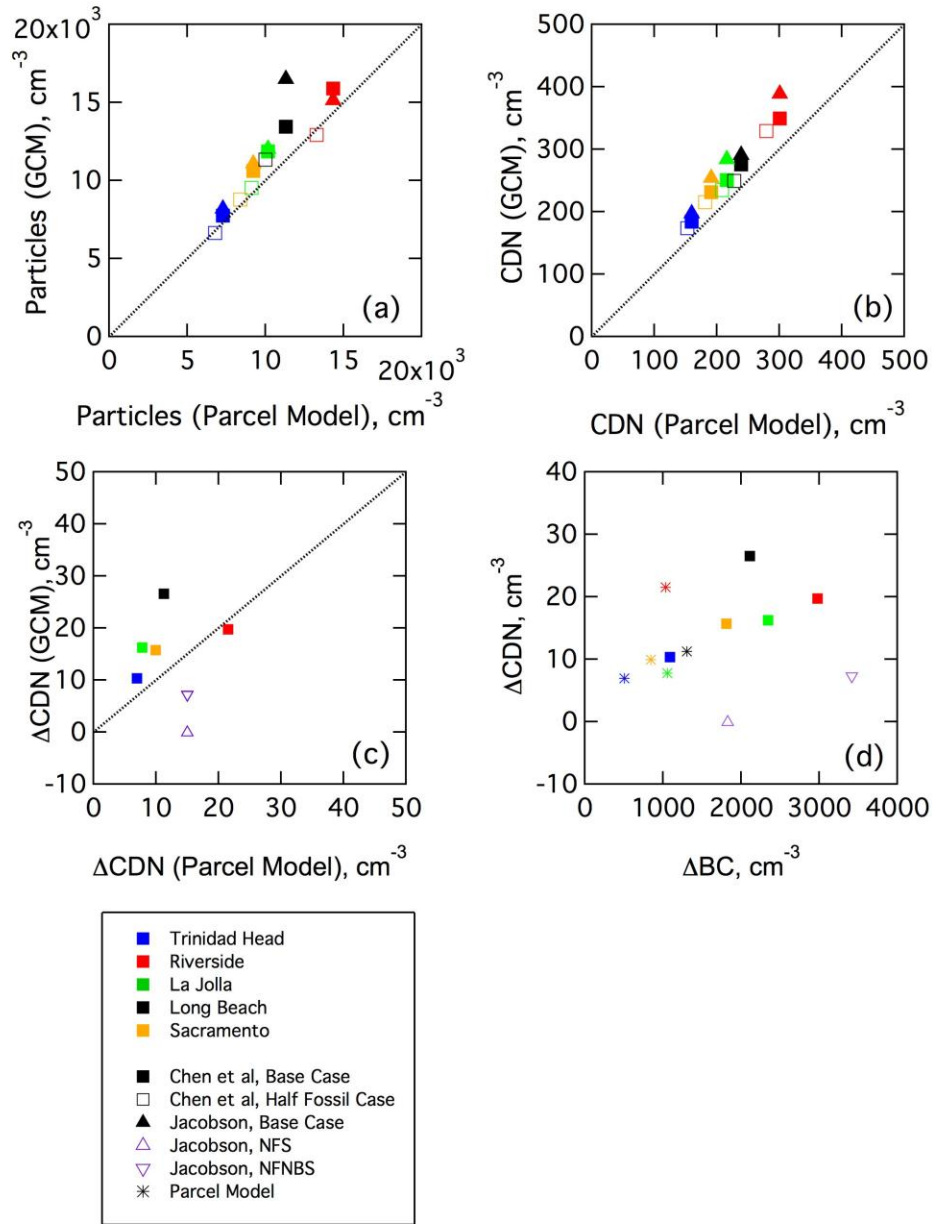


Figure 0.2: Comparison of (a) total particles, (b) activated cloud droplet number, (c) change in the droplet concentration (defined as base case-BC mitigation case), and (d) dependence of change in droplet number on change in BC-type particle number from this study.

Conclusions: We find the chemically detailed particle distributions from field campaigns to be very comparable to the emission inventory-based particle concentrations used in GCMs. The particle number size distributions agree well for the three model types. BC particles in the parcel model are smaller than the

GCMs possibly because the locations and seasons of the field campaigns did not represent the entire particle sources included in the GCMs.

The parcel model simulated a simple cloud layer that was consistent with typical stratocumulus observations common in California, while incorporating accurate kinetic activation of cloud droplets. In the polluted California environment, BC-type particles contribute between 14% and 18% of the total cloud droplets, agreeing reasonably well with GCM predictions for California. The parcel model predicted that BC mitigation reduces the droplet population in clouds by between 5% and 9%, with a corresponding increase in mean droplet size. This result agrees well with predictions for the half fossil fuel case from the *Chen et al.* [2010a] model (with a smaller relative magnitude). The predicted decrease in CDN by these two models differs from the *Jacobson* [2010] model which found that fossil soot mitigation (in isolation from biomass burning soot) caused a 1% increase in CDN concentration. This difference was likely the result of that model's treatment of fossil fuel BC particles as initially hydrophobic, although its inclusion of semi-direct and cloud absorption feedbacks could have also reduced CDN by reducing cloud supersaturation.

The reduction in CDN in California due to the decrease in activated BC particles supports the possibility that the cloud albedo effect of BC particles may partially offset the direct forcing reduction, especially in regions where BC mitigation targets fossil fuel sources.

Future Work: A complete understanding of the climate impacts of BC mitigation in California and the rest of the world (including processes such as the impact on sea ice and land glaciers) requires further work to reduce the uncertainty associated with indirect effects. In this report we presented several chemically different scenarios for BC found in California that resulted in potentially different cloud impacts. Future mitigation studies should incorporate and consider the hygroscopicity of BC (due to varied sources) when estimating aerosol effects. While the scope of this work was limited to determining the impact of BC on cloud droplet number and size, future work is needed extending this study to estimate the actually forcing impact through radiative transfer calculations.

Once these further issues are addressed, reducing BC emissions will have important implications beyond California. Since atmospheric transport of pollutants (including BC) means that impacts of emission changes in California will be felt downwind by other states and regions, controlling BC will have important impacts that extend beyond California itself. The prevention of additional warming by direct effects of BC would be shared by other states and countries. New satellite measurements may even be able to detect these impacts, if BC reductions in California precede those elsewhere, as improved retrievals of aerosol and cloud properties over land may be able to detect BC reductions. Furthermore, if we improve the representation of BC in climate

models, then California and other states will be able to design more effective control strategies to minimize climate change and its impacts.

1.0 INTRODUCTION

1.1 Motivation

Black Carbon, or BC, is a major component of aerosol particles that is generally related to combustion sources such as automobile exhaust and biomass burning [Andreae and Merlet, 2001]; yet the effects of BC remain a wildcard in assessing the impacts of aerosols on climate change. BC is ubiquitous: recent studies show that 10% to 80% of the submicron particle number size distribution measured in Mexico City were primarily black carbon or contained black carbon [Moffet *et al.*, 2008]. BC's light absorbing and myriad chemical properties enhance its contribution to visibility degradation, change in the earth's radiation budget, and health risks from air pollution. Recent research has also shown that BC contributes to the accelerated melting of snow and ice in the poles and mountain glaciers through the reduction in snow albedo [Hansen and Nazarenko, 2004]. Studies show that BC in Arctic snow increases the absorption of shortwave radiation by 5-10% compared to soot-free snow [Clarke and Noone, 1985]. This increase in sensible heat at the surface is compounded by heating of the atmospheric boundary layer as well.

Ramanathan et al. [2007] showed that the atmospheric heating related to BC is of the same magnitude as greenhouse gases over the Himalayas and regional scales as large as the Indian subcontinent. Due to its short atmospheric lifetime, BC is not globally mixed and reductions in BC emission the low hanging fruits for slowing down global warming in the coming decades. However, unlike ozone or carbon dioxide for which strict chemical definitions and measurement standards are clear, black carbon is chemically ambiguous and operationally defined. While this shortcoming in no way minimizes the importance of black carbon for climate and air quality, it does mean that monitoring and mitigating it will be subject to a series of technical and legal challenges.

While BC has been found to contribute to the warming of the atmosphere due to direct solar absorption, it may also play a role in cooling through its contribution to cloud-active aerosols and changes in cloud microphysical properties [Roberts *et al.*, 2003a]. The BC impact on clouds manifests in three principle ways: i) BC inclusion inside a cloud drop (or ice crystal) enhances solar absorption (and leads to positive forcing), because the radiation field inside a drop is enhanced by multiple scattering. ii) Nucleation of additional cloud drops by BC leads to more drops enhancing albedo of clouds and leading to negative forcing (cooling effect). iii) If the cloud water content is unchanged the drop size will decrease with increased production of drops and this will enhance cloud life-time and lead to further enhancement in cloud albedo and negative forcing. Cloud-process (i), known as cloud-inclusion effect will enhance atmospheric heating; while processes (ii) and (iii), known as indirect effects, will enhance surface dimming. Finally, the heating of the atmosphere is increased by the direct forcing and the cloud-inclusion effect, then the boundary layer relative humidity drops, and this

evaporates the clouds leading to additional heating (the semi-direct effect). A complete understanding of the climate consequences of BC mitigation requires the relative quantification of these effects.

1.2 Prior Work

Predicted effects of black carbon forcing vary widely (see Figure 1) as global climate models suggest a negligible climate forcing to one of the same order as greenhouse gases with as much as 0.3–0.4°C warming [Chung and Seinfeld, 2005]. The emission reduction of particulate BC plus associated OM may slow global warming more than may any emission reduction of CO₂ or CH₄, since it has been estimated that eliminating all BC and OM could eliminate 20-45% of net warming within 3-5 years [Jacobson, 2001]. Many uncertainties regarding the role of black carbon particles on climate remain, especially in emission-up climate studies where the quantity and spatial distribution of black carbon in the atmosphere depend on rates of emission and removal or scavenging. Bond *et al.* [2004] presents the most recent comprehensive black carbon emission inventories for the world. This inventory considers fuel type, combustion conditions, and emission controls, which result in difference from previously published estimates [Penner *et al.*, 1994] in global black carbon emissions by a factor of two. The discrepancy between the modeled and actual emissions is not known; but is likely to be even more pronounced at the local scales. The rate of removal of black carbon depends on atmospheric processes that change the hydrophobicity of soot. For instance, hygroscopic coatings have been shown to increase the probability for wet removal and scavenging of black carbon particles in the laboratory [Popovicheva *et al.*, 2008; Zuberi *et al.*, 2005], but field measurements have shown their lifetimes to be longer than organic carbon [Lim *et al.*, 2003], highlighting the importance of observing the degree to which black carbon is mixed with other compounds.

Due to uncertainties in emission rates and atmospheric processes, recent GCM studies that have investigated the indirect effects of BC on CDN concentrations differ not only in magnitude, but also in the sign of the change in cloud droplet concentrations [Bauer *et al.*, 2010; Chen *et al.*, 2010a; Koch *et al.*, 2009; Kristjansson *et al.*, 2005; Spracklen *et al.*, 2011]. A recent multi-model comparison [Koch *et al.*, 2011] investigating the effect of soot mitigation on liquid clouds concluded that soot removal could either increase or decrease the cloud droplet number with the final response depending on a combination of factors including the composition and size of the soot particles, the magnitude of soot change caused by emissions reduction, as well as the non-linear response of the indirect effect itself. Although some generalized trends were found among the GCMs investigated, there was no consensus on the sign or magnitude of the cloud response in isolation to soot emission mitigation. In particular, Chen *et al.*, [2010a] estimated that a 50% reduction in fossil fuel emissions would result in a 6% decrease in the globally-averaged CDN concentration as a consequence of the first indirect effect; Jacobson [2010], who performed climate response

simulations, reported a 1% increase in cloud droplet number concentration for complete removal (100% decrease) of fossil fuel soot emissions (but a 10% decrease when both fossil fuel and biomass burning emissions were removed). The increased drop concentration of *Jacobson* [2010] in the no fossil soot (NFS) simulation was the combined result of the modeled hydrophobicity of fossil fuel BC particles and the changes in cloud dynamics from semi-direct and cloud absorption effects of BC on temperature.

1.3 Research Objectives

The primary objective of this study is to assess the importance of the first indirect effect (albedo effect) of black carbon on radiative forcing of the Earth's atmosphere by an intercomparison of a detailed chemical-microphysical model to the parameterizations embedded in global model simulations. The models used in this study are constrained and initialized by field measurements selected to represent aerosols founds in different ambient conditions in California. By utilizing measured aerosol properties we eliminate any uncertainties introduced in GCMs due to emission inventories and atmospheric processes. The mitigation scenarios proposed for BC reflect the observed trends in California BC reported by *Bahadur et al.* [2011].

1.4 Structure of Report

The overall research objective of this work was accomplished by the completion of four specific tasks that are discussed in detail in the following chapters.

Task 1: Analysis of available measurements and identification of BC chemical case studies. Results from this task are described in Chapter 2.

Task 2: Scenario model runs and analysis of results. Results from this task are described in Chapters 3 and 4.

Task 3: On-site meeting with advisors and comparisons to GCMs. These results are described in Chapter 5.

Task 4: Significance of Results and Sensitivity Studies. These results are summarized in Chapter 6.

In addition to including these results in this final report, we prepared, submitted for peer-review, and published the conclusions of this work in the article titled "Importance of composition and hygroscopicity to the effect of BC mitigation on cloud properties: Application to California Conditions" in the *Journal of Geophysical Research* (volume 117: D09204, 2012, doi:10.1029/2011JD017265).

2.0 California Aerosol Case Studies (Task 1)

2.1 Introduction

With respect to elemental carbon (EC) and black carbon terminology, estimates of BC and EC are made with a variety of instrumentation and measurement techniques. This has also resulted in a variety of definitions related to chemical and/or physical particle properties, intended applications, and the different measurement and estimation approaches, and has given rise to an array of descriptive terms such as “graphitic carbon”, “elemental carbon”, “black carbon”, and “soot” which are used interchangeably with black carbon in the literature. The chemical definition of black carbon is the fraction of carbon-containing compounds that, in addition to elemental carbon (EC), are co-emitted in combustion (as “soot”) or are measured to be light-absorbing at wavelengths relevant to the Earth’s incoming or outgoing radiative balance. The fraction of BC that is not EC is chemically defined to be organic carbon (OC) – the term associated with compounds that contain carbon atoms bonded to hydrogen atoms, and possibly a variety of other non-carbonaceous atoms. Because BC includes both EC and OC (and typically excludes carbonate, a third form of carbon-containing compounds), techniques that measure elemental composition are insufficient to chemically separate BC. As a result, some chemical methods typically identify OC and EC rather than BC, using methods that separate these carbonaceous compounds by their combustion or volatilization temperature of the carbon fraction and associated changes in their light absorbing content. One example of such methods is Evolved Gas Analysis (EGA) with thermo-optical corrections for charring.

Recent advances have provided other methods to separate a fraction of OC that is associated with EC and is inferred to be BC, in the sense of being co-emitted with soot; these include spectroscopic and mass spectrometric techniques. Both single-particle and ensemble-aerosol mass spectrometers, including the ATOFMS as well as the Aerosol Mass Spectrometer (AMS, Aerodyne Inc.) have used characteristic elemental and mass fragments to identify the organic components associated with EC. In addition, Fourier transform infrared (FTIR) spectroscopy has been used to identify organic sources that are associated with EC. These methods incorporate clustering or factorization methods to separate particle and OC types. In California, measurements of OC, EC, and BC from prior campaigns have provided multiple constraints on the chemical and physical properties of black carbon in the atmosphere.

ATOFMS has been used to identify BC-containing particles from carbon fragments in a variety of locations in California, providing a rich data set for model comparison. This technique uses C-containing fragments to identify a clear spectral signature in individual particle measurements above and below 1 μm in diameter. Figure 2.1 illustrates examples from available field

measurements of the internal mixing state using ATOFMS single particle measurements, and details of the field campaigns are summarized in Table 2.1.

Location	Campaign	Dates	Coords. (N, W)	Environment	Refs.
Trinidad Head (TH)	CIFEX	4/1-4/23 2004	41.3, 124.9	Clean marine, long-range pollution	[Holecek et al., 2005]
Riverside, (RV)	SOAR I	7/22-8/15 2005	33.5, 117.2	Highly polluted urban and regional transport	[Shields et al., 2008]
La Jolla (LJ)	Mobile Study	12/13- 12/19 2006	32.5, 117.1	Polluted urban and biomass burning	
Long Beach (LB)	LABMS I	8/15-9/7 2007	33.5, 118.9	Polluted marine and urban mix	[Ault et al., 2009]
Sacramento (SA)	CARES	6/2-6/28 2010	38.3, 121.2	Polluted urban and long range transport	

Table 2.1: Selected sampling sites and dates for field measurements in this study.

2.2 Representative Case Studies

We have compiled black carbon measurements available in the California domain between 2001-2010 in conjunction with Dr. Ramanathan's ARB project (08-323), which encompass the following data sets:

- a. IMPROVE measurements of EC and total aerosol mass in remote locations. Aerosol phase measurements are available in 22 locations in California for this time period, which we downloaded and resolved into monthly averaged data.
- b. STN (EPA) measurements of EC and total aerosol mass in urban areas. Measurements from this network are available from 19 sites, we have downloaded this data and resolved it into monthly averages similar to the IMPROVE measurements. Validation of EPA EC measurements with collocated Aethelometer measurements show a deviation at higher concentrations, suggesting that further quality control and screening of outliers may be required.
- c. ATOFMS measurements from ground-based field projects in Riverside (SOAR-I and SOAR-II), La Jolla, Long Beach, and Trinidad Head (CIFEX), and aircraft measurements based in Sacramento (CARES) provided by Dr. Kimberly Prather. These ATOFMS measurements are available for limited time periods but are used in this study to constrain the number of BC-containing particles, since the IMPROVE and EPA measurements are mass-based.

We have used the ATOFMS identification of BC-containing particle number measurements to initialize the aerosol-cloud interaction parcel model to

evaluate the impact of BC containing aerosols on clouds in California. We used IMPROVE and STN-EPA measurements to constrain and compare the total EC mass concentrations as determined from the field studies and climate models as a check on the total aerosol mass. Based on ambient environment, we designated the case studies at Trinidad Head (2001) to represent clean environments, Riverside (2005) and Sacramento (2010) to represent polluted urban environments, Long Beach (2007) to represent polluted marine environments, and La Jolla (2006) representing an environment influenced by biomass burning events including the *Shekell*, *Westside*, and *Sequoia* fires in Southern California (between December 3 – December 10), and 309 acres of open biomass burning in San Diego County [www.wildfirezone.org].

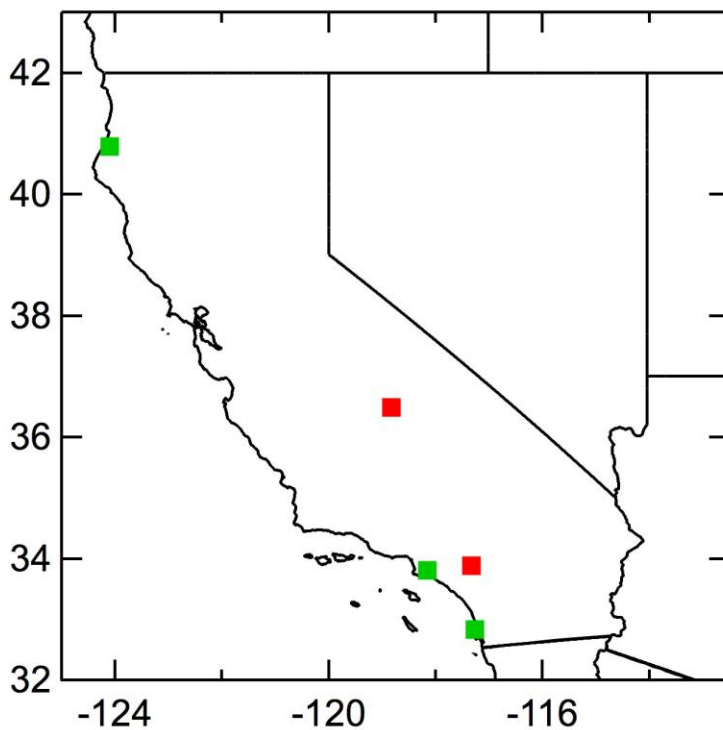


Figure 2.1: Locations of field campaigns with available ATOFMS aerosol measurements chosen to represent different ambient conditions in California.

2.3 Determining External Mixing State of Aerosol

To characterize the external mixing state of aerosols (i.e. mixing between particles of different chemical compositions) we relied on statistics determined from ATOFMS field studies that have been conducted to characterize external mixtures of aerosol particles in California. ATOFMS enables online size-resolved chemical characterization of ambient aerosol samples through information about the chemical fingerprints associated with each particle type [Silva and Prather,

1997; *Silva et al.*, 1999; *Suess and Prather*, 1999]. The chemical characteristics of submicron carbonaceous aerosol particles have been established based on a previous comparative study [*Bahadur et al.*, 2010], and here we use a similar methodology to describe the aerosol observed at different field sites. To obtain a consistent distribution of aerosols at all field sites, we describe all measured aerosols as an external mixture of four major particle types:

- (a) The Black Carbon (BC) type is characterized by a positive ion mass spectrum that is dominated by carbon atom clusters (C_n) with smaller signal contributions from organic carbon, nitrate, sulfate, and ammonium tracer fragments. The mass spectra are similar to spectra of particles sampled during source tests from vehicular exhaust [*Sodeman et al.*, 2005], suggesting that these particles are produced from primary sources of fossil fuel combustion and correspond most closely to atmospheric black carbon.
- (b) The Organic Carbon (OC) type is characterized by major OC peaks at +27 (C_2H_3) and +43 (C_2H_3O), a peak at +39 (K) associated with organics produced during biomass combustion, and positive ion fragments up to and beyond +150 indicative of high mass compounds that may be formed via atmospheric processing [*Silva et al.*, 1999].
- (c) The Sulfate-type particles are characterized by a large peak at -97 (HSO_4) in the negative ion spectrum. These particles also contain some BC and OC fragments, indicating an internal mixture.
- (d) Similar to the sulfate-type, the Nitrate-type particles contain a large peak at -62 (NO_3) in the negative spectra. The nitrate and sulfate particles are often internally mixed; in these cases the particle is classified as either sulfate or nitrate according to the larger peak.

We classified the particles sequentially in the order described (i.e. BC type, OC type, Sulfate type, and Nitrate type) to avoid any double counting, since as indicated particles belonging to one type may contain some tracer fragments associated with the other types due to internal mixtures.

The sulfate and nitrate particle types typically do not produce positive ion spectra but are still likely to contain a carbonaceous core [*Pratt et al.*, 2010], consistent with their formation via condensation of secondary species on to a core possibly generated from combustion sources. We found some spectra containing sea salt peaks in the coastal sites – these were typically mixed with the sulfate and nitrate classes. Pure sea salt particles do not make up a significant fraction of the total submicron particles at these sites, and we exclude it as an externally mixed particle type, although we do allow for some internal mixing with sea salt. Between 5% and 10% of particles at each site did not fall into the four categories; these particles were classified as “other” and not included in our analysis of BC impact on clouds.

2.4 Determining Aerosol Size Distribution

Since the ATOFMS samples single particles, the instrument cannot determine a chemically-resolved total size distribution for ambient aerosols. In order to constrain aerosol size distributions at the field studies, we used the following algorithm: First, the relative concentrations of the particle types described in Sec 2.3 was determined by analyzing the ATOFMS measurements (using a nozzle inlet with a cutoff of 3 μm) within the ensemble of sampled particles. Since the instrument detected larger particles with higher efficiency than smaller particles, unscaled number counts [Allen *et al.*, 2000; Bhave *et al.*, 2002] could not be directly summed up to recreate the ambient size distribution. In the second step, we used measurements from three co-located sizing instruments – Scanning Mobility Particle Sizer (SMPS, 0.01-1 μm), Optical Particle Counter (OPC, 0.5-2.5 μm), and Aerodynamic Particle Sizer (APS 1-25 μm) to determine the absolute aerosol number concentration between 0.01 and 2.5 μm .

At each field campaign, a period of 24 hours was chosen to evaluate the size distribution in order to eliminate spikes in concentration due to any diurnal variation and localized high emission events. Instead, the average of all size distributions measured over this period was assumed to represent the site. In the final step, we assumed that the relative fraction of each particle type within 0.1 μm size bin as determined from the ATOFMS was statistically similar to that found in the ambient and constructed a relative size distribution (independent of absolute particle counts) for the four different particle types. In the final step, we multiplied the total particle count (from sizing instruments) with the particle-type fractions (from the ATOFMS) to reconstruct the representative atmospheric number size distribution. The size-dependent relative ATOFMS particle fraction and corresponding reconstructed number size distributions are illustrated in Figure 2.2 for the five sites and the total particle number resolved by external mixing type are listed in Table 2.2.

Location	Total aerosol particles, cm^{-3}	BC type, cm^{-3}	OC type, cm^{-3}	Sulfate type, cm^{-3}	Nitrate type, cm^{-3}	Other/Not resolved cm^{-3}
Trinidad Head (TH)	7287	1015	4526	820	483	442
Riverside, (RV)	14321	2130	9136	1419	902	734
La Jolla (LJ)	10178	2112	5794	1532	511	229
Long Beach (LB)	11295	2656	6499	1168	578	394
Sacramento (SA)	9231	1686	5939	808	157	622

Table 2.2: Total number of aerosol particle types resolved by external mixing state measured using ATOFMS and particle sizing instruments.

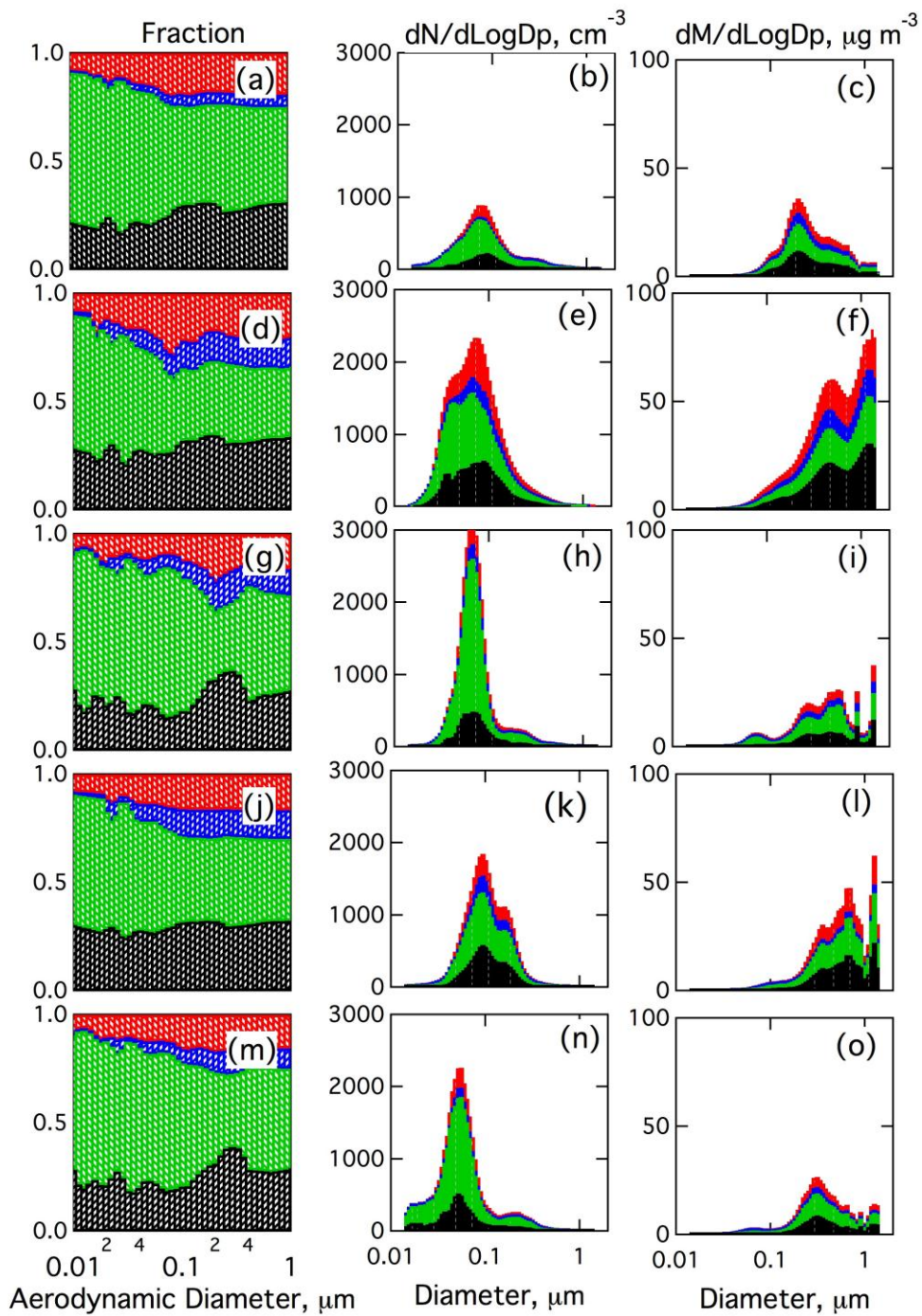


Figure 2.2: Distributions of the Sulfate (red), Nitrate (blue), OC (green) and BC (black) particle types determined at the field sites included in this study. The first column illustrates normalized fractions from the ATOFMS, the second column illustrates number size distributions from the sizing instruments, and the third column illustrates the corresponding mass size distribution. Panels are from (a-c) Trinidad Head, (d-f) Riverside, (g-i) Long Beach, (j-l) La Jolla, and (m-o) Sacramento.

2.5 Determining Internal Mixing State

As described in Section 2.3, while the ATOFMS can identify chemical components of a particle from tracer fragments, it cannot evaluate their relative abundance. In order to fully utilize the chemical resolution of the aerosol-cloud interaction model, we treated each of the four particle types as an internal mixture of five species – ammonium sulfate, ammonium nitrate, BC (represented as elemental carbon), OC (represented as a long chain carboxylic acid [Russell *et al.*, 2011]), and sea salt (represented as sodium chloride). Allowing for internal mixtures allows the representation of carbonaceous cores in the sulfate and nitrate particle types, and increased the addition of highly hygroscopic secondary species to the carbonaceous particles. Characteristic densities for the four externally mixed particle types have been measured [Qin *et al.*, 2006] and densities of the pure components are available from laboratory measurements. These densities are summarized in Table 2.3. We used the volumetric mixing rule from equation 2.1 to constrain the internal mixing state of each of the major particle types, such that

$$\rho_{obs} = \sum_i f_i \rho_i \quad 2.1$$

where ρ_{obs} is the observed density of the aerosol particle type, f_i is the fraction of the pure species within that type and ρ_i is the pure component density.

Aerosol Particles		Pure Species	
Type	Measured Density, g cm ⁻³	Component	Measured Density, g cm ⁻³
BC	2.0	BC	2.2
OC	1.9	OC	0.8
Sulfate	1.7	Ammonium Sulfate	1.8
Nitrate	1.9	Ammonium Nitrate	1.7
		Sodium Chloride	2.1

Table 2.3: Measured aerosol particle and constituent component densities used to determine internal mixing state.

Since multiple solutions of Equation 2.1 are possible, the internal mixing state represents a possible composition rather than a unique one. Figure 2.3 illustrates the calculated composition of each of the four particle types that are used to represent the particle populations observed in this study. Since this method only constrains the internal mixing state rather than providing an exact solution, there exists a range of possible compositions. The range of possible internal mixing

state for each of the particle types and principal chemical species is tabulated in Table 2.4

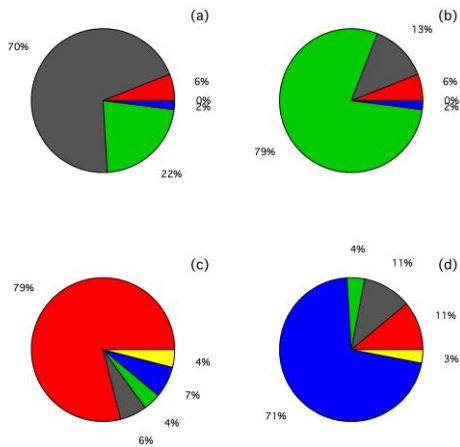


Figure 2.3: Internal mixing state of the (a) BC Particle type, (b) OC Particle type, (c) Sulfate Particle type, and (d) Nitrate Particle types used in this study. The mass fractions of the pure components are illustrated as BC (grey), OC (green), Ammonium Sulfate (red), Ammonium Nitrate (blue), and Sodium Chloride (yellow).

Particle Type	BC	OC	Ammonium Sulfate	Ammonium Nitrate	Sodium Chloride
BC Type	0.70 (0.65-0.83)	0.22 (0.17-0.24)	0.06 (0.03-0.08)	0.02 (0.01-0.04)	0.0 (-)
OC Type	0.13 (0.09-0.17)	0.79 (0.72-0.85)	0.06 (0.03-0.07)	0.02 (0.01-0.03)	0.0 (-)
Sulfate Type	0.06 (0.03-0.08)	0.04 (0.02-0.06)	0.79 (0.73-0.88)	0.07 (0.03-0.09)	0.04 (0.02-0.06)
Nitrate Type	0.11 (0.04-0.13)	0.04 (0.02-0.06)	0.11 (0.03-0.12)	0.71 (0.68-0.76)	0.03 (0.02-0.06)

Table 2.4: Average fraction and possible range of compositions for the internal mixing state of the aerosol particle types using five constituent species measured in this study.

2.5 Conclusions

In order to characterize aerosol-cloud interactions in California, we have identified five field campaigns in California that represent a variety of ambient conditions with the most complete available chemical and physical measurements of externally mixed particles; the sites are: Clean Marine (Trinidad Head), Polluted Urban (Riverside and Sacramento), Polluted Marine (Long Beach), and Biomass Burning dominated (La Jolla). For each of these case studies we obtained

ATOFMS measurements of the size resolved single particle measurements that provide the internal chemical mixing state of the different types of aerosol particles. Based on chemical tracer analysis we have used these measurements to classify the aerosol particles as being EC dominated (from fossil fuel combustion), OC dominated (from secondary organic condensation and biomass burning), and Sulfate/Nitrate dominated (from SO_2/NO_x chemistry).

In order to determine the ambient aerosol distributions, we have also obtained co-located SMPS and APS measurements of the number size distributions of the aerosol particles. These measurements provide the total number size distribution of the principal aerosol types in conjunction with ATOFMS statistics. We have obtained density measurements of the chemical particle types identified by the ATOFMS from literature based on laboratory studies. Finally, we have synthesized these three sets of measurements to describe the aerosol particles to initialize their physical (size and mass) and chemical (both internal and external mixing states) properties in the aerosol model for each site.

3.0 Microphysical Aerosol-Cloud Modeling Approach (Task 2)

3.1 Introduction

In order to quantify the first indirect effect of BC mitigation in California, we need to determine the total cloud droplet number (CDN) and mean droplet size that are associated with measured aerosol distributions under both the baseline and mitigation scenarios. One source of uncertainty in calculating CDN changes and subsequent indirect effects in large scale GCMs is the introduction of parameterizations to reduce computational time [Meskhidze *et al.*, 2005]. While these parameterizations capture the cloud microphysics and dynamics on some scale, they cannot describe the influences of size and chemically resolved aerosol distributions on the cloud drop spectrum. Furthermore, since parameterizations typically do not resolve mixtures of masses of different chemical species within droplets, they cannot unambiguously describe the influences of the mitigating any one component, such as BC [Erlick *et al.*, 2001].

Instead, we employ a parcel model that connects detailed cloud chemistry and microphysics with a calculated supersaturation profile [Guibert *et al.*, 2003; Snider *et al.*, 2003]. The ability to keep track of particle size and composition during cloud evolution, while limiting the scale to a localized aerosol parcel, allows us to evaluate the importance and influence of different aerosol types and microphysical parameters. Since such parcel models do not include the feedback of BC on the temperature profile, the semi-direct effects are not assessed in this study.

3.2 Aerosol-Cloud Parcel Model

The aerosol model of Russell and Seinfeld [1998] is a parcel model embedded into a vertical profile of meteorological conditions (temperature, pressure, and relative humidity) that predicts the growth of aerosol populations for explicit external and internal mixtures of aerosol species, accounting for coagulation, condensation, deposition, activation, and nucleation. For non-water components, both particle number and mass are conserved as particles grow. During coagulation events, the identity of the aerosol particles remains with the involatile core. The aerosol populations are described by both external mixtures (that can differ in size distribution), and internal mixtures of typical atmospheric components including BC, OC, Ammonium Sulfate, Sodium Chloride, and Water.

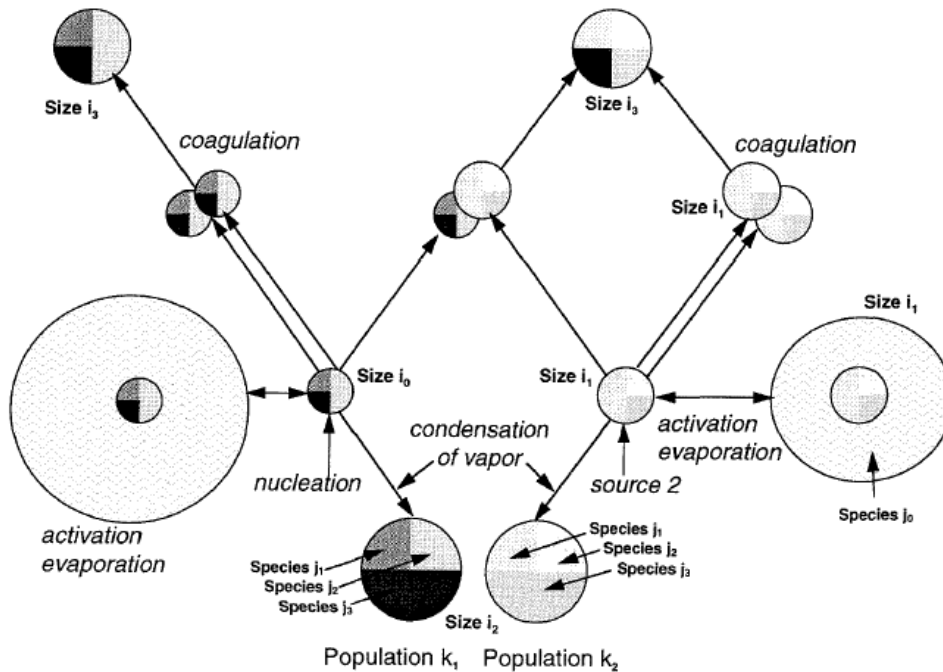


FIGURE 1. Diagram of mechanisms of particle dynamics described by the proposed algorithm.

Figure 3.1: Aerosol-Cloud interaction processes included in the parcel model (from Russell and Seinfeld [1998]).

A systematic representation of the processes involved in tracking the multiple aerosol distributions under conditions of changing supersaturation is illustrated in Figure 3.1. The gas phase and heterogeneous sulfur chemistry are also described explicitly in the model but are negligible in the short simulations conducted for this work. Water is treated in a moving section representation allowing for the accurate calculation of evaporation and condensation depending on the relative humidity, and both the aerosol mass and particle number concentration are tracked using a dual moment method. The maximum supersaturation, CDN concentration, and equivalent cloud droplet radius are calculated kinetically based on the detailed chemical composition of each particle type and size rather than from equilibrium Köhler theory, providing a more flexible treatment of warm stratus clouds where the time scale for change of supersaturation can be comparable to or smaller than the time scale for particle growth.

Specific features of the sectional model include –

1. **External Mixtures:** The model structure is designed to be able to account for independent particle populations in an external mixture. This feature provides the ability to track particle nuclei through condensational and coagulative growth so that the source of particle number can be identified directly rather than from deductions based on particle mass. Since particle number is the property that determines

many aerosol properties, such as cloud droplet concentration in the atmosphere, this model provides the ability to assess the role of aerosol sources in the indirect effect of cloud properties on radiation.

2. Aerosol Dynamics: Both the aerosol number and mass are treated independently, with differential equations describing the rate of change in both, integrated at each time step. By using a two-moment approach, changes in mass and number are calculated separately for both coagulation and condensation. In condensation no new particles are added but mass is added to preexisting particles. In coagulation, particles are lost from two sections, and gained by another section; the mass lost corresponds exactly to the number lost, but the mass gained may be a fraction of the number gained since the new particle may not correspond to an existing sectional diameter. The population identity of particles after coagulation and condensation is retained by the characteristic involatile core (such as sea salt or EC), using the volatility of particle components to provide a preference order. Conservation of mass and number provide constraints during coagulation and condensation.
3. Conservation of Number: Since the number distribution of particles determines the number of nuclei available for cloud droplet formation, conservation of particle number in calculation of growth and coagulation is an important feature in determining aerosol cloud interactions. The approach taken here utilizes results of a recent comparison of zero and higher order methods for solving the condensation equation.
4. Condensation of Water: Condensation of a vapor under supersaturated conditions is treated as a dynamic process. In this work water is treated as the condensate but other vapors can also be substituted. Growth due to condensation of non-supersaturated solutes is calculated using fixed sections. Growth of particles by addition of water does not alter the fixed sectional size or the dry diameter, instead water condensation is calculated using a moving sectional approach.
5. Particle Sources: Particle and vapor sources are parameterized from field measurements.
6. Particle Activation in Clouds: The water content of particles under subsaturated conditions is assumed to be in local equilibrium with the ambient environment. The time required to reach this equilibrium is a function of humidity, temperature, solute activity, and number concentration (typically 0.1s under ambient conditions). Under supersaturated conditions the time required to reach water equilibrium is significantly longer than that under subsaturated conditions (typically 1 s). Since this time is longer than the rate of change of supersaturation, equilibrium is not assumed under supersaturated conditions, and the amount of water condensed is calculated kinetically.

More detailed descriptions of the model are available in the literature [Russell and Seinfeld, 1998; Russell et al., 1999]. In order to place results from the sectional model in context we also compare them to results obtained from current state of the art GCM simulations. We have compared our parcel model results with the global model runs of GISS-TOMAS [Adams and Seinfeld, 2002; Chen et al., 2010a] and GATOR-GCMOM (Gas, Aerosol, Transport, Radiation, General Circulation Mesoscale and Ocean Model) [Jacobson, 2010] models.

3.3 GISS-TOMAS Model

The GISS-TOMAS model [Chen et al., 2010a; Chen et al., 2010b] tracks the size-resolved mass and number aerosol concentrations and number concentrations of CCN in a global domain using a geographical resolution of 4° latitude x 5° longitude. The size-resolved TOMAS microphysics module simulates aerosol number concentration, size distribution, composition, and CCN online within the GISS GCM II community model. The module tracks both the number and the mass of aerosols in each size bin in the aerosol distribution. A sectional approach is applied to define the boundaries of 30 size bins (spanning approximately dry diameters of 0.01 to 10 μm), in terms of dry aerosol mass. Microphysical processes include coagulation, condensation/evaporation, nucleation, and in-cloud sulfur oxidation. Sulfate is assumed to exist as ammonium bisulfate and to be internally mixed with sea salt.

The Nenes-Seinfeld activation parameterization is applied online to compute nucleation scavenging of aerosol and number concentrations from the aerosol simulation. The cloud droplet number is determined by the maximum supersaturation, which is controlled by the water vapor balance and is obtained by classifying droplets by proximity to their critical diameter (“population splitting”). A fixed cloud base updraft velocity of 0.6 m s^{-1} over land and 0.3 m s^{-1} over ocean is prescribed, giving optimal closure between observations and theory for cloud droplet calculations in cumulus and stratocumulus clouds. The effective water vapor uptake coefficient is set to 0.06. The model was integrated for 2 years with present-day emissions of sulfur and sea salt and monthly, grid-by-grid CCN spectra are derived from the simulations of the second year.

In the BASE simulation, emissions from fossil fuel and biofuel sources are based on the emissions inventory of Bond et al. [2004], and biomass burning emissions are from the online GFED inventory. In the mitigation scenarios, both the mass and number of emitted carbonaceous aerosols are reduced from their respective sources by 50%, under the assumption that the size distribution remains invariant.

3.4 GATOR-GCMOM model

GATOR-GCMOM [Jacobson 2010] is a one-way-nested (feeding information from coarser to finer domains) global-regional Gas, Aerosol, Transport,

Radiation, General Circulation, Mesoscale, and Ocean Model that simulates climate, weather, and air pollution on all scales. The universal treatment of feedbacks in the model to determine climate response obviates the need to calculate radiative forcing, which induces error (a) by requiring meteorology to be identical for two simulations, thereby preventing feedbacks from occurring when one component is removed and (b) by requiring different forcings to be calculated separately for different feedbacks, which induces error through the assumption that radiative forcings for different processes are linearly additive.

Aerosol processes included anthropogenic and natural emissions, binary and ternary homogeneous nucleation, condensation, dissolution, internal-particle chemical equilibrium, aerosol-aerosol coagulation, aerosol-hydrometeor coagulation, sedimentation, dry deposition, and transport. The model treats two discrete aerosol size distributions, each with 14 size bins (2 nm to 50 nm in diameter), and three hydrometeor distributions, each with 30 size bins (0.5 mm to 8 mm in diameter) (Table 1). The two aerosol distributions included an emitted fossil-fuel soot (EFFS) and an internally mixed (IM) distribution. EFFS particle sources include vehicles, power plants, industry, ships, and aircraft. IM particle sources included biofuel burning, biomass burning, the ocean (sea spray, bacteria), soils (dust, bacteria), volcanoes, and vegetation (pollen, spores). Particle number and mole concentrations of several chemicals are tracked in each aerosol size bin and in each hydrometeor size bin of each size distribution. The components within each bin of each distribution are internally mixed in the bin but externally mixed from other bins and other distributions fitted to initial log-normal distributions.

Emissions for biomass burning are those averaged over 5 years for which burn data were available (2002–2006). In the model, the five year cycle was repeated. For biofuel burning, the spatial distribution of black carbon (BC) and primary organic carbon (POC) emissions from Bond et al. [2004] were used, but the global fuel burn rate was increased by scaling with the 2009 to 1995 world population change. Coarse-particle emissions were 0.25 of fine BC and 0.45 of fine POC. The CO₂ emissions are biofuel combustion emissions, not combustion minus regrowth emissions, as the model calculated photosynthesis online, accounting for biofuel regrowth.

The model treats first and second indirect aerosol effects on clouds explicitly and together with cloud radiative effects. Multiple subgrid cumulus clouds are treated along with grid-scale stratus clouds in each column. Cumulus and stratus thermodynamics were constrained by the quasi-equilibrium assumption; all cloud and precipitation microphysics was time-dependent, explicit, and size- and composition-resolved [Jacobson 2010].

3.5 Inclusion of Nitrate Equilibrium

As part of the effort in this project we have modified the microphysics model developed by Russell and Seinfeld to incorporate three additional nitrate species (Ammonium Nitrate, Sodium Nitrate, and Nitric Acid) that are present in significant concentrations in California aerosol measurements. Thermodynamic equilibrium properties for the $\text{NH}_4^+\text{-NO}_3^-\text{-SO}_4^{2-}\text{-H}^+$ and $\text{NH}_4^+\text{-NO}_3^-\text{-SO}_4^{2-}\text{-Na}^+\text{-Cl}^-$ systems are calculated using the equations developed as part of the community AIM model (<http://www.aim.env.uea.ac.uk/aim/aim.php>) developed for extended inorganic/organic interactions. The details of thermodynamic parameters and equations are provided by *Clegg et al.* [1998]. We have performed a series of sample simulations using monomodal mixtures with different modal radii and calculated hygroscopic growth curves for Ammonium Sulfate and Ammonium Nitrate using the expanded model. The growth curves show the expected deliquescence transition and compare well with experimental data. The Sulfate growth curve is illustrated in Figure 3.2 and the Nitrate growth curve is illustrated in Figure 3.3.

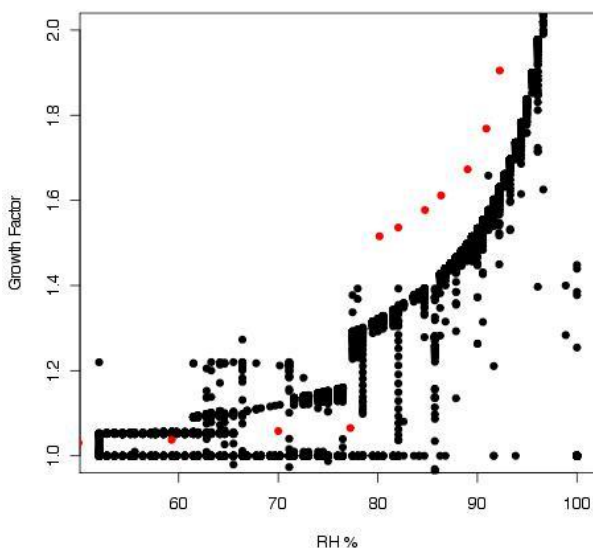


Figure 3.2: Hygroscopic growth curves for Ammonium Sulfate particles in a Sulfate-Nitrate mixture determined from the aerosol parcel model. Red Dots indicate laboratory measurements [*Svenningsson et al.*, 2006].

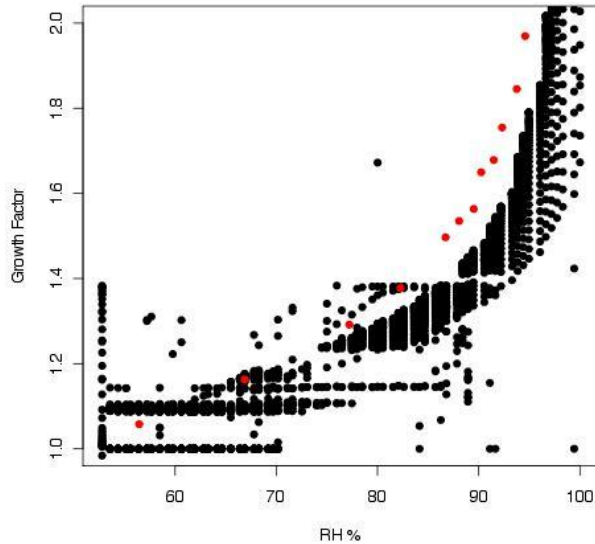


Figure 3.3: Hygroscopic growth curves for Ammonium Nitrate in a sulfate-nitrate mixture determined from the aerosol parcel model. Red dots indicate laboratory measurements [Svenningsson *et al.*, 2006].

The Sulfate growth curve shows the following features: (1) a size dependence of the HGF, (2) the growth factor varies between 1.2 and 2.0 and is smaller than laboratory measurements, and (3) activation of all particles occurs between 78% and 84% RH, typically slightly after the bulk deliquescence value of 80% because of the finite time steps used in the calculation.

Similarly, compared to laboratory measurements, the Nitrate growth predicted by the model shows the following features: (1) the growth factor varies between 1.4 and 2.0, which is very comparable to laboratory measurements, (2) variations in the growth factor are higher than those observed for sulfate type particles, (3) activation of all particles occurs between 70% and 76% (also slightly higher than the theoretical deliquescence value of 68% due to the finite time steps of the calculation).

3.6 Allowing Variable Updraft

The baseline version of the model assumes constant thermal equilibrium between the aerosol parcel and the ambient air (i.e. parcel temperature is equal to the ambient temperature as a function of altitude). A fixed updraft velocity is then applied to the aerosol enabling interaction with the cloud deck. We have modified the parcel model to create a second mode of operation where the aerosol temperature varies adiabatically as latent heat of water condensation and expansion are released. Additionally, the parcel is allowed to entrain moist air. In this mode of operation, the updraft velocity varies in order to maintain hydrostatic equilibrium. The advantage is that we do not have to rely on a pre-assumed

updraft velocity and the total energy is conserved in the aerosol packet, more closely modeling reality.

The calculated updraft mode follows the treatment of [Pruppacher and Klett, 2003] developed for convective clouds, calculating the updraft velocity at each time step while allowing the adiabatic cooling of the aerosol parcel and entrainment of humid air. The changes in temperature and updraft velocity that are evaluated simultaneously are

$$dT = -\left(\frac{gUdt + L\Delta w + \phi[L\Delta w + c_p(T - T_a)]}{c_p}\right) \quad (1)$$

$$dU = \left[\frac{2g}{3}\left(\frac{T - T_a}{T_a} - w\right) - \frac{2\phi}{3}U^2\right]dt \quad (2)$$

where T is the parcel temperature, T_a is the ambient temperature, g is the acceleration due to gravity, w is the liquid water mixing ratio, L is the latent heat of condensation of water, c_p is the specific heat of water, ϕ is a dimensionless entrainment parameter computed based on the liquid water profile determined using a fixed updraft velocity, t is time, and U is the updraft velocity.

3.7 Modeling Meteorological Conditions

We have used a continentally-influenced marine stratus cloud to represent clouds interacting with the aerosols in this study. Profiles of meteorological variables that were collected on a flight of the Monterey Area Ship Track (MAST) experiment on JDT 178 [Durkee *et al.*, 2000] in a continentally-influenced cloud layer from 173 to 405 m above sea level are used to describe the temperature profile, humidity profile, and total amount of available liquid water. The total available water vapor in the cloud is 0.35 g m^{-3} and the cloud base temperature is 285.3 K. The frequent presence of low lying stratocumulus clouds off the coast of California, particularly in the spring and summer months [Lu *et al.*, 2007], suggests that this is a reasonable and relevant cloud thermodynamic structure that can be applied to the case studies considered here, as the measurements were all made in coastal, or near-coastal sites. The temperature and RH profile used in this study is illustrated in Figure 3.4.

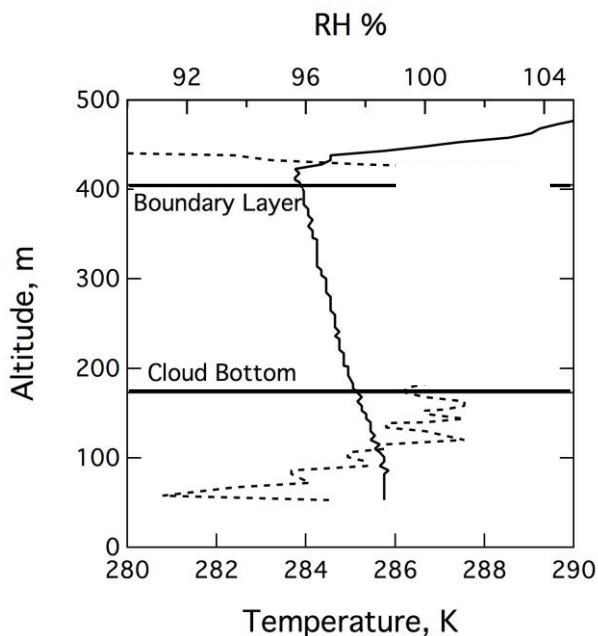


Figure 3.4: Observed temperature (solid line, bottom axis) and RH from dewpoint hygrometer (dashed line, top axis) profiles of the model stratocumulus cloud used in this study to represent common California conditions. (RH values in cloud are not available because the dew point hygrometer does not function above saturation.)

3.8 Conclusions

We have used the detailed aerosol-cloud interaction model developed by Russell and Seinfeld [1998] to study the first indirect effect of aerosols (including BC) in California. We have extended the model in two ways as a part of this study – first, we have expanded the number of available chemical species to include Nitrate compounds, and second, we have introduced an adiabatic constraint that allows the updraft velocity to vary as the aerosol interacts with ambient air. In order to represent simplified ambient conditions, we have set up a scenario describing idealized cloud-aerosol interactions in California by constructing temperature and humidity profiles that describe a continentally influenced marine stratus cloud based upon offshore measurements.

4.0 Model Scenario Runs – Base and Mitigation Cases (Task 2)

4.1 Introduction

To quantify the first aerosol indirect effect from the clouds formed by BC CCN, we have analyzed the five chemically resolved case studies described in Chapter 2 with the standard set of meteorological conditions described in Chapter 3. For each chemical case study, we have determined the aerosol and cloud droplet size distributions before and after cloud processing of the aerosol parcel. Each of these chemical case studies has been repeated for 50% and 90% reductions in BC in order to establish the effect of mitigation scenarios. The differences among these case studies represent the role of BC particles in cloud droplet formation in conditions that represent California.

4.2 Baseline Simulations

We have used the parcel model in conjunction with the measured aerosol size distributions described in Chapter 2 to establish baselines for conditions commonly seen in California under a variety of emission scenarios. The model was operated in the calculated updraft mode and truncated after one complete cloud cycle following which the CDN population was calculated. The simulated parcel altitude, relative humidity, liquid water content, and updraft velocity for the five case studies for the baseline cases is illustrated in Figure 4.1.

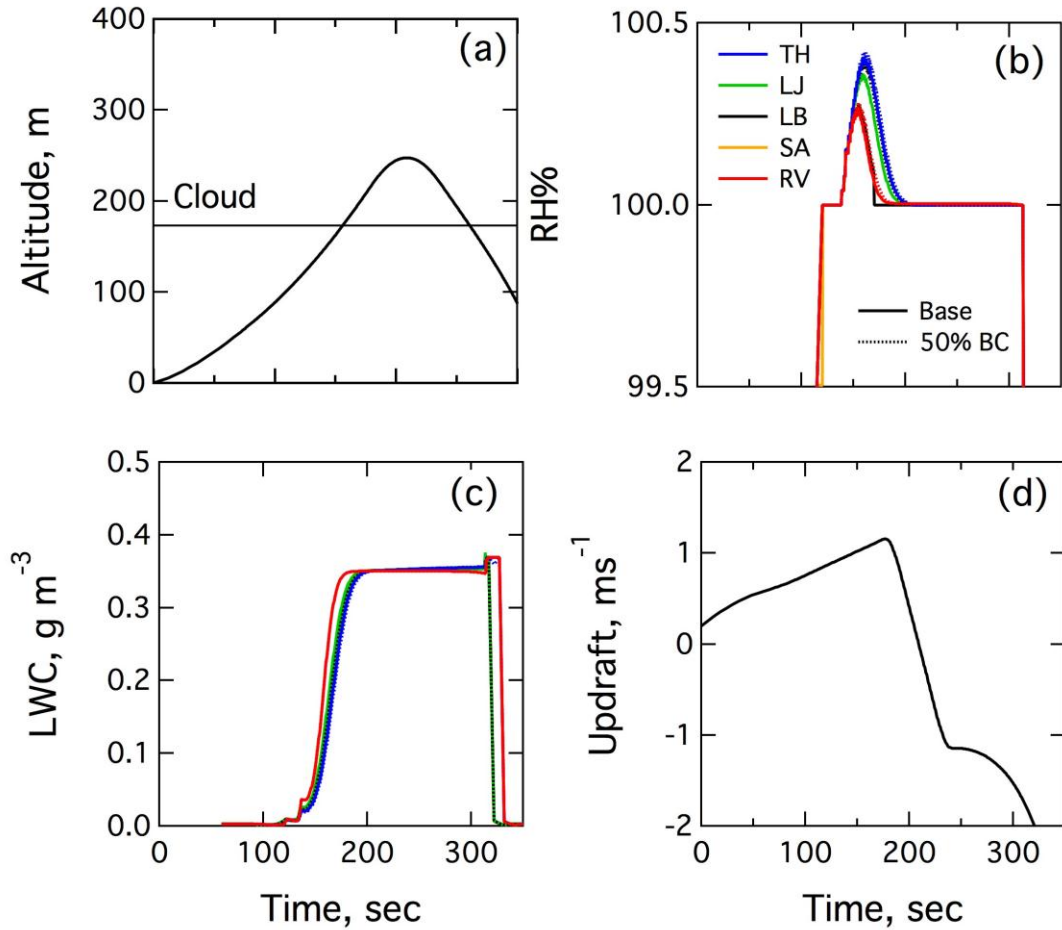


Figure 4.1: Parcel model simulations of the (a) Altitude, (b) RH, (c) liquid water content, and (d) updraft velocity for TH (blue), RV (red), LJ (green), LB (black), and SA (orange) baseline simulations over a single cloud cycle.

For each of the simulations, we initialized the model with the aerosol parcel at rest ($U=0$) at sea level with a potential temperature 1K in excess of the measured atmospheric temperature. Due to this excess temperature (or heat), in the first stage of the simulation, the parcel was warmer than the surrounding air and accelerated upwards. As the air parcel ascended it was cooled due to adiabatic expansion, reaching a temperature first equal to, and then less than, the surrounding air. The parcel attained a maximum updraft velocity ($U=1.4\ m\ s^{-1}$ for the conditions simulated here) before starting to decelerate. In the second stage of the simulation (starting at approximately 150 s), the parcel entered the supersaturated region and the available water vapor started to condense onto the cloud condensation nuclei (CCN). The supersaturation reached a maximum value (between 0.24 % at RV and 0.38 % at TH) and then started to drop as the water vapor condenses. In the third stage of the simulation (starting at approximately 220 s), the aerosol had sufficiently decelerated and had a negative velocity and started to descend, eventually leaving the cloud. In the fourth and final stage of the simulation (starting at approximately 310 s), the aerosol parcel

descends through the unsaturated layer below the cloud, and rapidly loses all condensed water. For the cloud used in this study, a single cloud cycle typically lasted 300 seconds of simulated time after which the simulations were terminated, *i.e.* the downdraft leg outside the cloud and loss of water were neglected. We found that this simulation time was sufficient for the parcel to achieve the maximum supersaturation, to condense the available liquid water, and to start to descend in the subsequent downdraft. The updraft velocity profiles are identical in all five cases, indicating that the small differences in the rate of water condensation in the different cases did not have an appreciable effect on the updraft velocity, since the difference in amount of latent heat released is relatively small. The total number of aerosol particles, BC type particles and corresponding cloud processed properties *i.e.* maximum supersaturation, maximum updraft velocity, and CDN for each of the baseline case studies are listed in Table 4.1.

4.3 Identification of Activated Droplets

One of the principal advantages of using a parcel model to investigate aerosol-cloud interactions is the ability to track chemically resolved size distributions in time as the aerosol undergoes cloud processing. Figure 4.2 illustrates the evolution of the BC particle size distribution at the start of the simulation, in-cloud, before maximum supersaturation, and in-cloud, after maximum supersaturation for the five case studies. As liquid water condenses onto the aerosol particles in the supersaturated region of the cloud, individual particles start to grow across the entire size distribution. In addition to increased modal diameter as a result of growth, we also find a secondary mode centered at approximately 10 μm (or larger). We have defined this secondary mode to be the activated mode [Cantrell *et al.*, 1999; Erlick *et al.*, 2001] representing cloud droplets and integrated the size distribution curve to determine the total number of cloud droplets formed and mean cloud droplet diameter. It is important to note that the cut-off diameter for the activated mode was identified from the number size distribution for each particle population following activation, and not pre-selected.

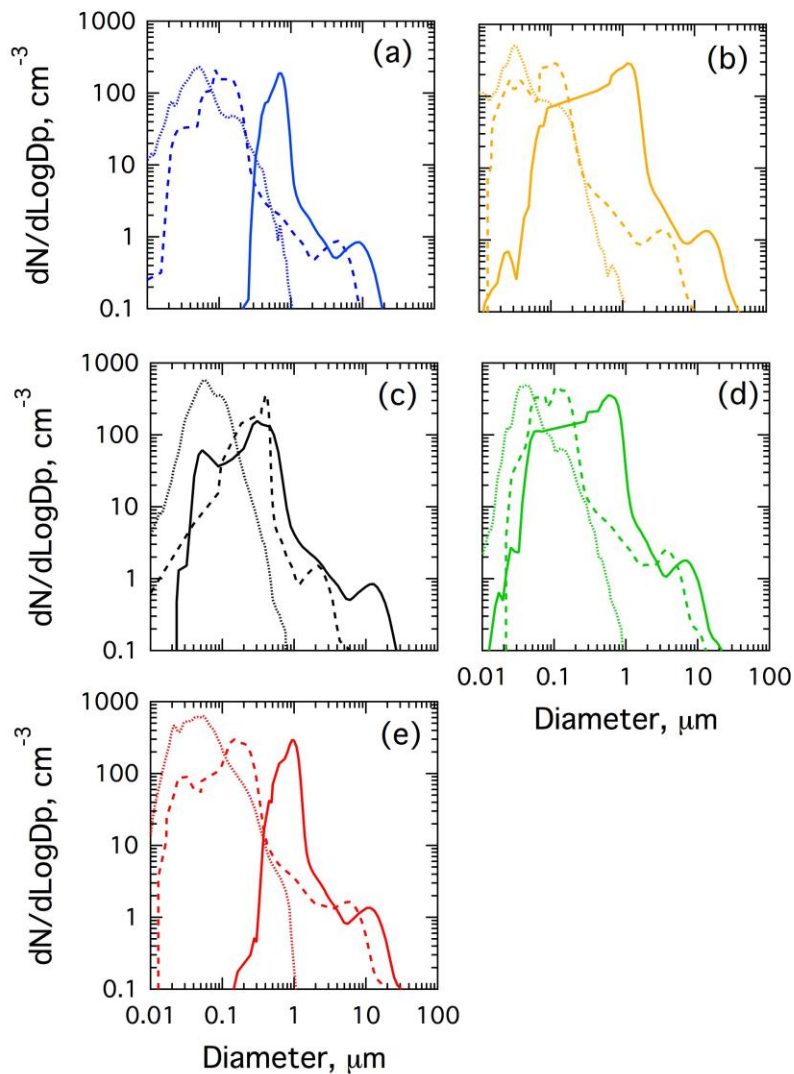


Figure 4.2: Parcel model simulations of the BC particle size distribution from (a) TH, (b) SA, (c) LB, (d) LJ, and (e) RV cases. Dotted lines are below cloud ($t=50$ s), dashed lines are in-cloud before max RH ($t=150$ s), and solid lines are in-cloud after max RH ($t=250$ s). Particles in the secondary mode around $10 \mu\text{m}$ are considered activated.

Location	N_a cm^{-3}	N_b cm^{-3}	N_c cm^{-3}	N_{bc} cm^{-3}	S_{\max} %	D_c μm	U (at S_{\max}) ms^{-1}
TH	7287	1015	160	31	0.38	9.8	0.92
RV	14321	2130	301	59	0.24	8.6	0.83
LJ	10178	2112	216	64	0.27	9.3	0.86
LB	11295	2656	289	111	0.25	8.7	0.86
SA	9231	1686	221	77	0.34	9.0	0.87

Table 4.1: The number concentration of the total aerosol particles (N_a), black carbon particles (N_b), cloud droplets (N_c), black carbon cloud droplets (N_{bc}), average cloud droplet diameter (D_c), maximum supersaturation (S_{\max}), and corresponding updraft velocity (U) for the five baseline case studies.

4.3 BC Mitigation Scenarios

To determine the impact of reduced BC on cloud droplet concentrations, we have repeated the model analysis using two mitigation scenarios, reducing the BC by 50% and 90% of the observed total. We constructed the mitigation scenarios by decreasing the number concentration of the BC-type particles by half (and to 10%) while preserving the shape of the size distribution, i.e. the number concentration in each size bin was scaled down equally. We rely on the underlying assumption that a reduction in BC emissions reduces the number concentration of BC-type particles but does not alter the mean size, since the particle size (and morphology) is likely to be related to emission source type only. The size distributions and mass of the other particle types are preserved as measured (including the small BC mass component). An associated effect of these scenarios is that the secondary species internally mixed with the BC-type particles (approximately 25% of the mass, primarily OC) are also mitigated, but this reduction is small compared to the total amount of OC, Sulfate, and Nitrate. We note that these mitigation scenarios do not represent true “bottom-up” calculations (as contained in GCM simulations) where aerosol concentrations are impacted through combined atmospheric transport and aging processes once emission fields are altered. Rather, these scenarios closely mirror the trends in aerosol concentrations reported by [Bahadur *et al.*, 2011] who found that surface BC concentrations in California have declined over the past 20 years, while OC, Sulfate, and Nitrate concentrations have remained stable.

The overall effect of BC reduction on the aerosol is a loss in mass between 0.16 and 0.29 $\mu\text{g m}^{-3}$ (at TH, which is the cleanest site) and between 0.50 and 0.90 $\mu\text{g m}^{-3}$ (at RV, which is the most polluted site). These reductions in turn correspond to a reduction of between 5% and 13% in particle mass, and between 7% and 19% in particle number concentration. Since BC is co-emitted with many other particle components in ambient conditions, it is likely that an actual reduction of BC emissions would also reduce the OC, nitrate, and sulfate particle types that

constitute the other particle types. In fact, all three of these particle types may have BC cores, but, as a first approximation, we have reduced only the BC particle types. The total aerosol and BC type number concentration, change in aerosol mass, and cloud properties for both the 50% and 90% BC mitigation scenarios are tabulated in Table 4.2.

4.4 Observed Trends

We find that several consistent trends are observed across sites for the baseline case studies. First, the number concentration of cloud droplets (between 160 cm^{-3} at TH and 301 cm^{-3} at RV) is directly correlated to the number concentration of aerosol particles (7287 cm^{-3} at TH and 14321 cm^{-3} at RV), while the average droplet diameter is inversely related. This indicates that a large number of potential CCN compete with each other under these polluted conditions. The total liquid water in the parcel in each simulation reaches the maximum available water from the cloud. Secondly, a higher maximum supersaturation (0.38% at TH) is attained with a corresponding higher updraft velocity (0.92 m s^{-1} at TH) at lower aerosol concentrations indicating that the maximum supersaturation is limited by the size of the CCN sink, and the faster condensation in the more polluted cases releases latent heat more quickly, balancing the available buoyant force and resulting in slower updraft velocities.

Location	N_a cm^{-3}	N_b cm^{-3}	N_c cm^{-3}	N_{bc} cm^{-3}	$-\Delta m$ $\mu\text{g m}^{-3}$ (%)	S_{\max} %	D_c μm	U (at S_{\max}) ms^{-1}
50 % BC Mitigation Scenario								
TH	6780	508	151	17	0.16 (6%)	0.40	10.2	0.92
RV	13286	1065	284	28	0.50 (7%)	0.25	9.8	0.83
LJ	9122	1056	202	31	0.28 (5%)	0.34	9.6	0.86
LB	9987	1328	246	55	0.31 (6%)	0.30	8.7	0.86
SA	8388	843	198	38	0.25 (7%)	0.38	9.1	0.87
90 % BC Mitigation Scenario								
TH	6374	102	140	3	0.29 (11%)	0.42	10.4	0.92
RV	12434	213	266	6	0.90 (12%)	0.28	10.1	0.83
LJ	8277	211	182	6	0.50 (9%)	0.35	9.8	0.86
LB	8925	266	210	11	0.56 (11%)	0.32	9.1	0.86
SA	7714	169	173	8	0.45 (12%)	0.40	9.2	0.87

Table 4.2: The number concentration of the total aerosol particles (N_a), black carbon particles (N_b), cloud droplets (N_c), black carbon cloud droplets (N_{bc}), change in total aerosol mass (m), average cloud droplet diameter (D_c), maximum supersaturation (S_{\max}), and corresponding updraft velocity (U) for the 50% and 90% BC Mitigation Scenarios.

We observed a more interesting trend when comparing the reduction in cloud droplet number concentrations in the 50% BC mitigation case to the base case. At all field sites, the BC particle type typically comprises approximately between 15% and 30%. For example, at Trinidad Head (TH), the total BC number concentration is 1015 cm^{-3} out of a total of 7287 cm^{-3} (14%), compared to 2656 out of 11295 cm^{-3} (23 %) at Long Beach (LB). OC type particles comprise typically 50% of total particles in each case, with the highly hygroscopic Sulfate and Nitrate types constituting the balance. In the mitigation scenarios, the number concentration of BC particles is reduced to 50% while preserving the rest - therefore BC reduction causes between 7% (at TH) and 11% (at LB) reduction in the total particle number concentration, from 7287 to 6780 at TH and 11295 to 9985 at LB respectively. The change at the other sites can be determined by comparing Na values between Tables 4.1 and 4.2.

In contrast to the change in total number concentration, which is directly proportional to the BC decrease, the decrease in number concentration of cloud drops however is only between 5% (from 160 to 151 cm^{-3} at TH) and 9% (from 289 to 246 cm^{-3} at LB). The change at the other sites can be determined by comparing Nc values between Tables 4.1 and 4.2. This decrease is disproportionately smaller than the change in total number concentration. We found that this trend was repeated in the 90% mitigation case as well. These results imply that in addition to the total size distribution, the differences in aerosol chemical composition between the various field studies were also a contributing factor to the differences in activation of cloud droplets, since the decrease in CDN is disproportionately smaller compared to the decrease in total aerosol number.

To resolve this “dampening” in the reduction of CDNs compared to the reduction in total aerosol number concentration, we examined the total particle number concentration and fraction of particles activated for the found chemically distinct particle types. The total number distribution of cloud droplets for the case studies resolved by the four externally mixed particle types is listed in Table 4.3 for the baseline cases and Table 4.4 for the BC mitigation cases. The total CDN and fraction of activated particles are illustrated in Figure 4.2 for each case study as a function of simulation time. We find in general that the OC particles comprise the largest fraction of the total droplets (between 42% at RV and 55% at TH) and the nitrate particles comprise the smallest fraction (between 8% at TH and 16% at LB) consistent with the relative abundance of these particle types. For the baseline cases, activated BC particles make up between 16% (at LB) and 20% (at TH) of the total cloud droplets. The combined number of cloud droplets from Sulfate and Nitrate type particles is higher than their relative abundance in the total aerosol concentration, indicating that they activate with a higher fraction than the OC and EC particle types. A much larger fraction (between 4% and 8%) of the more hygroscopic nitrate and sulfate particles activate compared to the less hygroscopic OC and BC particles (between 1% and 3%). The fraction of each particle type is activated is listed in Table 4.3 – as can be seen across the

case studies, the OC type composed of long chain hydrocarbons contributes the largest total number of CDN but the smallest activation fraction (since the OC type also comprise the largest fraction of total particles). In the BC mitigation cases, the total number concentration of activated BC droplets decreases proportionately (as expected) by 50% and 90%, reflecting the decrease in number of total BC particles. We find however this decrease in CDN is balanced to a certain extent by a small increase in the number concentration of activated particles from the other species – for example, at TH the number of activated Nitrate+Sulfate particles increases to 71 cm^{-3} in the 50%BC case and 73 cm^{-3} in the 10%BC case compared to the base concentration of 67 cm^{-3} . A larger increase to 72 cm^{-3} and 78 cm^{-3} compared to the base concentration of 62 cm^{-3} is found at LB for Sulfate+Nitrate particles. These increases partially offset the decrease in BC type CDNs.

Location	Total	BC-type	OC-type	Sulfate type	Nitrate type
Cloud Droplet Number, cm ⁻³					
TH	160	31	62	36	31
RV	301	59	105	69	68
LJ	216	64	69	48	35
LB	289	111	118	32	28
SA	221	77	91	38	15
Fraction Activated					
TH	0.02	0.03	0.01	0.04	0.05
RV	0.02	0.03	0.01	0.04	0.07
LJ	0.02	0.03	0.01	0.03	0.06
LB	0.03	0.04	0.02	0.02	0.04
SA	0.02	0.05	0.02	0.04	0.05

Table 4.3: Total number of activated cloud drops and fraction of total particles activated resolved by particle type for the baseline cases.

We explain this “rebound” in the number of CDN as follows – as we noted in Section 4.2, due to the large number of potential CCN in the polluted continental air sampled here, the limiting factor for cloud droplets appears to be the total amount of available liquid water. As the number of BC particles is reduced in the mitigation scenarios, a larger number of the more hygroscopic sulfate and nitrate particles are able to compete for the available water than was previously associated with BC. The climate implication of this result is that if only BC particles are reduced (in polluted environments), the many CCN that do not contain BC still activate in place of the BC aerosol particles preserving, to some extent, the cloud droplet populations and mean diameters. Even though the decrease in CDN is much less than proportional to the BC reduction (due to an associated increase in the number of activated non-BC particles), the net effect of BC reduction is a small net decrease in the total CDN concentration.

Location	Total	BC-type	OC-type	Sulfate type	Nitrate type
50 % BC Mitigation: Cloud Droplet Number, cm ⁻³					
TH	151	17	63	38	33
RV	284	28	112	79	75
LJ	202	31	75	56	41
LB	246	55	119	38	34
SA	198	38	96	44	20
90 % BC Mitigation: Cloud Droplet Number, cm ⁻³					
TH	140	3	64	39	34
RV	266	6	106	73	71
LJ	182	6	76	58	43
LB	210	11	121	41	37
SA	173	8	92	40	17

Table 4.4: Total number of activated cloud drops activated resolved by particle type for the 50% and 90% Mitigation cases.

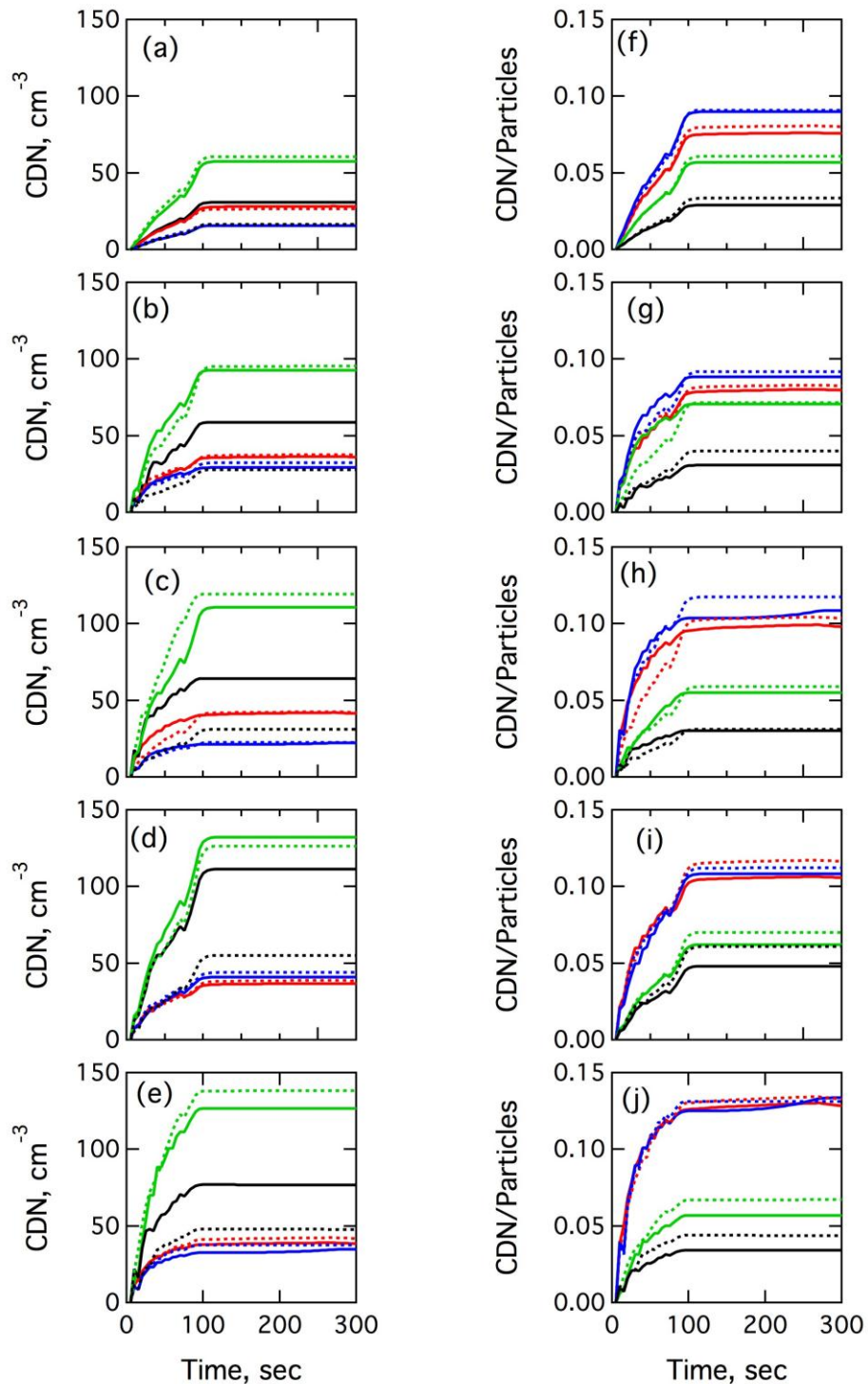


Figure 4.3: Parcel model simulations of the (a-e) cloud droplet number concentration and (f-j) fraction of particles activated for externally mixed particle populations corresponding to BC-type (black), OC-type (green), Sulfate-type (red), and Nitrate-type (blue) particles for a single cloud processing cycle. The base (solid lines) and 50% BC mitigation (dashed lines) cases are illustrated for (a),(f) TH, (b),(g) RV, (c),(h) LJ, (d),(i) LB, and (e),(j) SA.

4.5 Conclusions

We have used our detailed parcel model in conjunction with observed cloud (temperature and RH) profiles and observationally constrained aerosol populations to analyze the evolution of aerosol number size distributions due to cloud processing for the California scenarios described in Chapter 2. Based on the evolution of aerosol number size distribution in the baseline analysis as water condenses onto aerosol particles, we have determined the total number of activated cloud droplets based on the growth of a mode at 10 μm . We have repeated the model analysis using scenarios constraining the BC dominated particle types to 50% and 90% of the measured population to determine the impact of BC mitigation on cloud droplet population. We find that there is a partial “rebound” effect in the mitigation scenarios where, BC reduction causes a smaller decrease in the total cloud droplet number. We attribute this to the increased activation in more hygroscopic sulfate and nitrate containing particles. Even though the decrease in CDN is not proportional to the BC reduction (due to an associated increase in the number of activated non-BC particles), the net effect of BC reduction is a small net decrease in the total CDN concentration.

5.0 Comparison to GCM Results (Task 3)

5.1 Introduction

As mentioned in Section 1.2, there exists a large uncertainty in both the magnitude (and sign) of the aerosol indirect effects modeled in the GCM community, raising concerns about the overall climate impact of BC mitigation. In this project we have constrained the impact of BC mitigation on CDN based on observational data representing California conditions. In order to place these results in context however, we also need to compare them to results obtained from current state-of-the-art GCM simulations to better understand the trends in aerosol and cloud drop concentrations. We have compared our parcel model results with the global model runs of GISS-TOMAS (a combination of Goddard Institute for Space Studies and Two Moment Aerosol Sectional models) [Adams and Seinfeld, 2002; Chen et al., 2010b] and GATOR-GCMOM (Gas, Aerosol, Transport, Radiation, General Circulation Mesoscale and Ocean Model) [Jacobson, 2010] models. We chose these models for comparison because they had completed BC-reduction experiments that suggested contrasting impacts on the cloud droplet concentrations. In making the comparisons between GCM and parcel model results, we note the following differences: (1) GCM aerosol concentrations are constrained by emission inventories, while the parcel model was initialized by observations of ambient concentrations, (2) GCM values represent a grid-cell average around the sampling site as opposed to the point measurements used to initialize the parcel model, and (3) GCM cloud droplets are based on predictive meteorological fields whereas we have used a single thermodynamic profile of a polluted stratocumulus cloud.

As part of the collaborative work funded by CARB, both Professors Seinfeld (Caltech) and Jacobson (Stanford), who were lead investigators in the GCM simulations, served as project consultants and advisors.

5.2 GISS-TOMAS results

In brief, the GISS-TOMAS [Chen et al., 2010a; Chen et al., 2010b] model tracks the size-resolved mass and number aerosol concentrations that are used to calculate cloud droplet concentrations using the parameterization of Nenes and Seinfeld [2003] with the kinetic modification [Fountoukis and Nenes, 2005] and a geographical resolution of 4° latitude x 5° longitude. For evaluating the aerosol indirect effect, changes to the cloud albedo and lifetime were calculated. Two different BC mitigation scenarios were considered – Half-Fossil (HF), where only fossil fuel emissions were reduced by half, and Half-Carbon (HC), where carbonaceous emissions from all sources were reduced by half compared to the control case. These two mitigation scenarios resulted in a decrease in the total aerosol number concentration of 4.2% (HF) and 4.9% (HC), which in turn caused a larger decrease of 5.9% (HF) and 9.8% (HC) in the cloud droplet concentration.

The modeled reduction in total clouds was found to have a net heating effect on the atmosphere, raising concerns that there might be offsets to the direct forcing climate benefits of BC mitigation.

5.3 GATOR-GCCM results

Jacobson [2010] used a global-to-regional scale nested model in which cloud microphysical processes (for liquid, ice, and graupel phases) were solved explicitly with size and composition resolution, while cloud thermodynamics were considered to be at quasi-equilibrium. Climate and air pollution processes were explicitly linked, with the universal inclusion of climate feedbacks eliminating the need for the calculation of radiative forcing. In the global scenario, two BC mitigation experiments were conducted – in the No Fossil Soot (NFS) scenario, all BC from fossil fuel emissions was eliminated, and in the No Fossil, Biomass Soot, and Biomass Gasses (NFSBSG) scenario all emissions from both fossil fuel and biomass burning were eliminated. The mitigation scenarios resulted in a decrease of 1.5% (NFS) and 2.0% (NFSBSG) in the aerosol number concentration, but produced contrasting results for the cloud droplet number. When only fossil fuel emissions were eliminated, the CDN increased by 0.8% globally but decreased by 8.8% when all carbonaceous emissions were decreased.

5.4 California Domain Simulations

In addition to detailed results from prior GCM simulations described in Sections 5.2 and 5.3, Professor Jacobson conducted a new set of simulations as part of this project in a nested California domain resolved at 0.15 degrees (~13 km) west-east x 0.2 degrees (~22.2 km) south-north. The GCM code was revised to account for several new cloud, aerosol, and radiative variables that can be plotted out at individual locations as opposed to grid cell averages. The new simulation for the nested California domain (including offshore California) in the global model was conducted using emission and climate scenarios representing 2007. Full BC mitigation studies were not conducted in the higher resolution California domain due to limited computational resources. This advantage of using results from the new set of simulations are twofold – (1) it allows for a direct comparison of GCM total aerosol and cloud concentrations with the observationally constrained base case, and (2) it allows for validation of GCM seasonal cycles and surface concentrations with ground data from co-located IMPROVE sites that were assimilated as a part of this project. The seasonal cycle for total cloud droplets and representative size distributions for total aerosol and BC particles from this simulation are illustrated for the SEQU site in California in Figure 5.1 as an example.

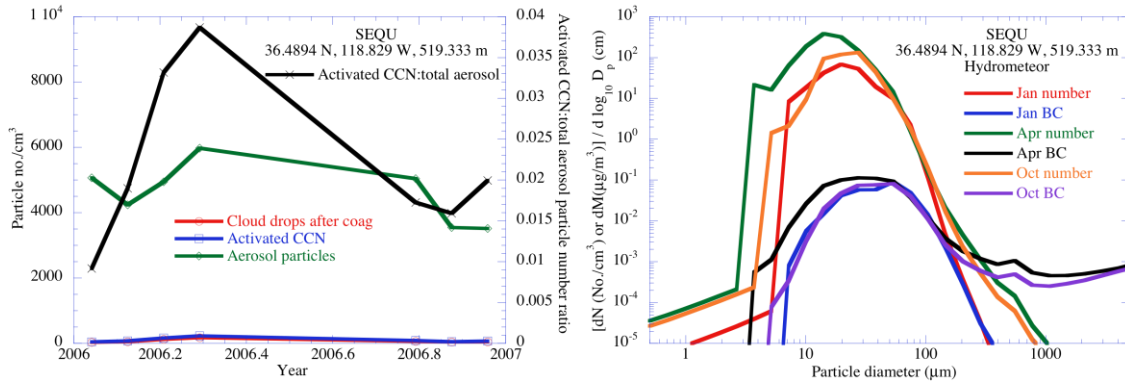


Figure 5.1: Representative CDN and aerosol size distributions from the nested California GCM year long simulation performed as a part of this work.

5.5 Validation with surface measurements

As described in Chapter 2, the measured aerosol mass distributions are not unique representations of ambient aerosols (since only the number concentrations are directly measured). To test the validity of our assumptions, and the GCM results for the nested California domain, we have compared the mass concentrations for sulfate, nitrate, BC, and OC, with ground measurements from the IMPROVE network. The nearly co-located IMPROVE sites selected for this validation are listed in Table 5.1. The speciated aerosol masses in this comparison represent PM_{2.5}. Figure 5.2 shows the comparisons of PM_{2.5} monthly averages measured from the IMPROVE sites, combined ATOFMS and particle number measurements, and calculated values from the GCMs of *Chen et al.* [2010b] (who do not explicitly report nitrate mass) and *Jacobson* [2010]. We find relatively good agreement between the four mass measurements, with the GCMs also successfully reproducing the annual cycles in EC, OC, and Sulfate. Compared to the IMPROVE measurements, the single-particle-based measurements for the parcel model under-predict the EC and Nitrate mass by between 10-15% and over-predict the OC and Sulfate mass by between 5-15%. This discrepancy is reasonable considering the variability associated with using nearby measurements, monthly averaged values, and the uncertainties associated with the measurements. Surface concentrations measured from the IMPROVE network are tabulated against GCM calculations and determinations from field measurements in Table 5.2.

Case Study	Location (N, W)	IMPROVE Station	Location (N, W)
Trinidad Head (TH)	41.3, 124.9	LAVO	40.5, 121.5
Riverside, (RV)	33.5, 117.2	SAGO	34.1, 116.9
La Jolla (LJ)	32.5, 117.1	JOSH	33.3, 116.3
Long Beach (LB)	33.5, 118.9	AGTI	33.4, 117.9
Sacramento (SA)	38.3, 121.2	BLIS	38.9, 121.1

Table 5.1: List of collocated IMPROVE network sites used for validating aerosol mass measurements from GCM calculations and observations used in this study.

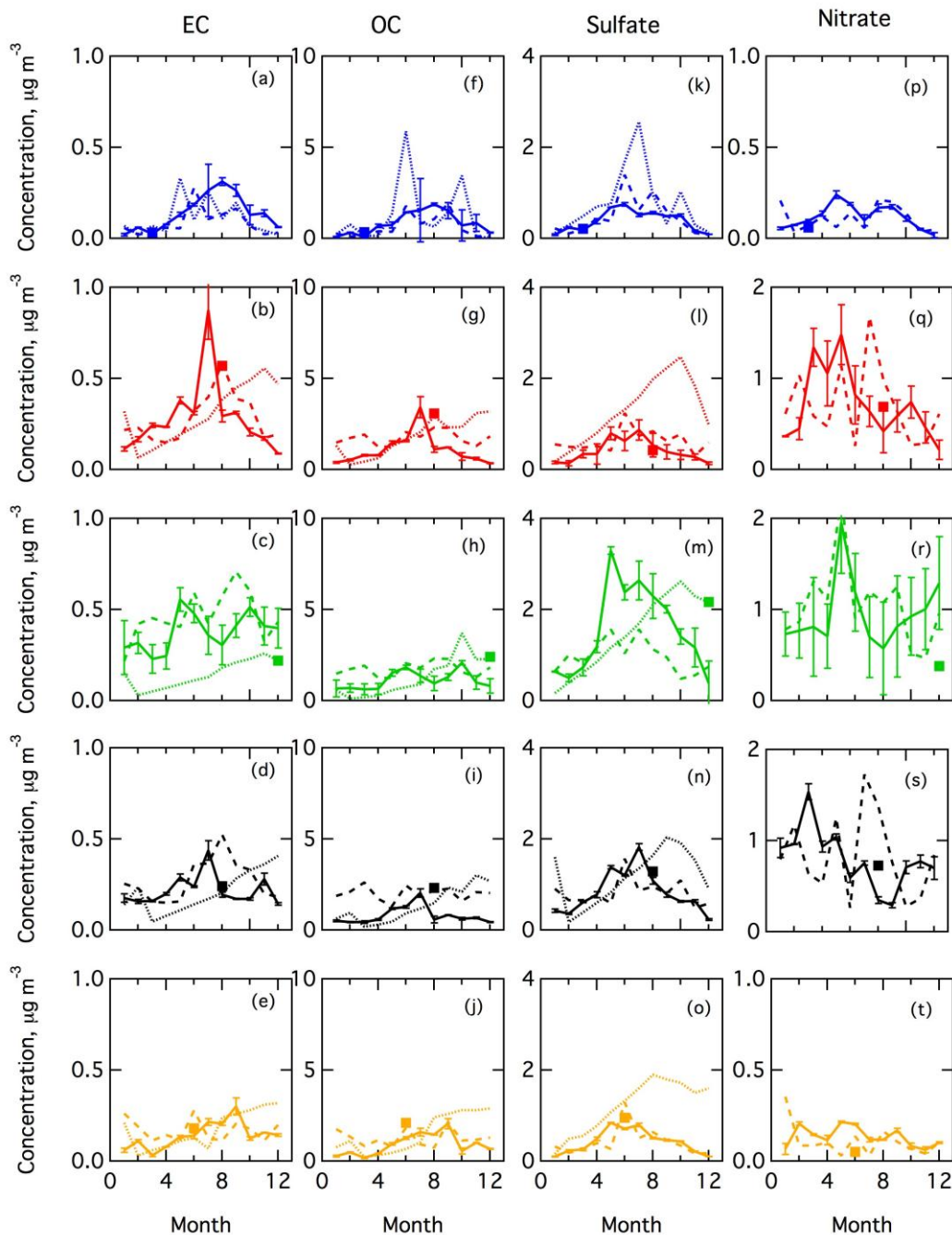


Figure 5.2: Monthly averages for the total PM_{2.5} mass concentration of (a-e) EC, (f-j) OC, (k-o) Sulfate, and (p-t) Nitrate at the TH (blue), RV (red), LJ (green), LB (black), and SA (orange) sites. Solid lines are filter based measurements from nearly collocated IMPROVE network sites at LAVO (blue), SAGO (red), JOSH (green), AGTI (black) and BLIS (orange). Dashed lines are from *Jacobson [2010]* and dotted lines are from *Chen et al., [2010a]*. Squares show monthly averages based on ATOFMS and particle size measurements used for initializing the parcel model. IMPROVE data is illustrated for 2006, with bars showing the 10 year variability from 2001-2010

Location	Month	Observationally based (this study)	Jacobson [2010] model	Chen et al. [2010a] model	IMPROVE
BC concentration, g cm ⁻³					
TH	Apr	0.03	0.06	0.04	0.08
RV	Aug	0.57	0.58	0.38	0.29
LJ	Dec	0.22	0.43	0.22	0.40
LB	Aug	0.24	0.52	0.20	0.19
SA	Jun	0.18	0.27	0.13	0.14
OC concentration, g cm ⁻³					
TH	Apr	0.35	0.38	0.13	0.69
RV	Aug	3.09	2.31	2.92	1.10
LJ	Dec	2.40	1.82	2.30	0.81
LB	Aug	2.32	2.18	1.48	0.58
SA	Jun	2.10	1.82	0.67	1.28
Sulfate concentration, g cm ⁻³					
TH	Apr	0.21	0.44	0.70	0.37
RV	Aug	0.43	0.84	1.98	0.53
LJ	Dec	2.17	0.75	2.16	0.38
LB	Aug	1.29	1.38	1.64	1.09
SA	Jun	0.95	1.29	1.32	0.71
Nitrate concentration, g cm ⁻³					
TH	Apr	0.06	0.12	-	0.14
RV	Aug	0.69	0.98	-	0.42
LJ	Dec	0.38	1.95	-	1.29
LB	Aug	0.72	0.95	-	0.35
SA	Jun	0.10	0.13	-	0.20

Table 5.2: Monthly mean mass concentrations of PM_{2.5} Aerosols from the IMPROVE network, GCM calculations and observations used in this study.

5.6 Comparison of baseline size distributions

Kinetic processes associated with cloud processing including coagulation and growth is typically sensitive to particle size distributions. We can expect therefore that a possible explanation for differing model calculations may be the aerosol size distributions used for initializing the models. We compare the total aerosol size distributions at the five California sites, illustrated in Figures 5.3 (a-c). We find that the GCM-simulated size distributions agree well with the measured size distributions in the 0.05 to 1 μm size range but are higher by a factor of approximately 5 in the ultrafine size range (below 0.1 μm diameter). Since the number size distribution can be dominated by a large number of very small particles in a polluted environment, this difference can be explained by the difference in the smallest size bins used across the models; these smallest particles however are unlikely to significantly impact the total aerosol mass and rarely activate to cloud droplets. The difference in size distributions between this work and the *Jacobson* [2010] model is more pronounced at larger sizes relative to the *Chen et al.* [2010a] model, particularly the supermicron coarse mode. This difference is likely due to the omission of large mineral dust (which was not quantified by the ATOFMS) in the parcel model. The absolute number of these coarse particles is small compared with the submicron particles so that they do not significantly impact CDN concentrations.

In addition to the total aerosol, we also compared the BC-type particle number size distributions as illustrated in Figure 5.3 (d-f). Here the difference is more pronounced than the total aerosols, with the BC particles in the *Jacobson* [2010] model being slightly larger compared to the other two distributions. This difference arises primarily from the differences in the simulation of BC particles from biomass burning. Both *Chen et al.* [2010a] and *Jacobson* [2010] find a larger decrease in the BC burden when the biomass burning emissions are reduced in addition to fossil fuel emissions consistent with BC in biomass burning processes. In this work, we classify particles dominated by secondary and biomass tracers in the OC category. Thus the BC particles we modeled are more representative of fresh fossil fuel emissions and are smaller compared with the GCMs.

Finally, Figure 5.3 (g-i) compares the size distribution of the total activated droplets from the baseline simulations (this size distribution was not computed in the *Chen et al.* [2010a] model that tracked the total water content and droplet number only). We find that both the modal diameter and total number concentration of cloud droplets agree well given the variety of differing assumptions in the three models, with particularly good agreement at the pristine TH location. The larger absolute number concentration of droplets from the GCM can be attributed to the higher particle number concentrations discussed above.

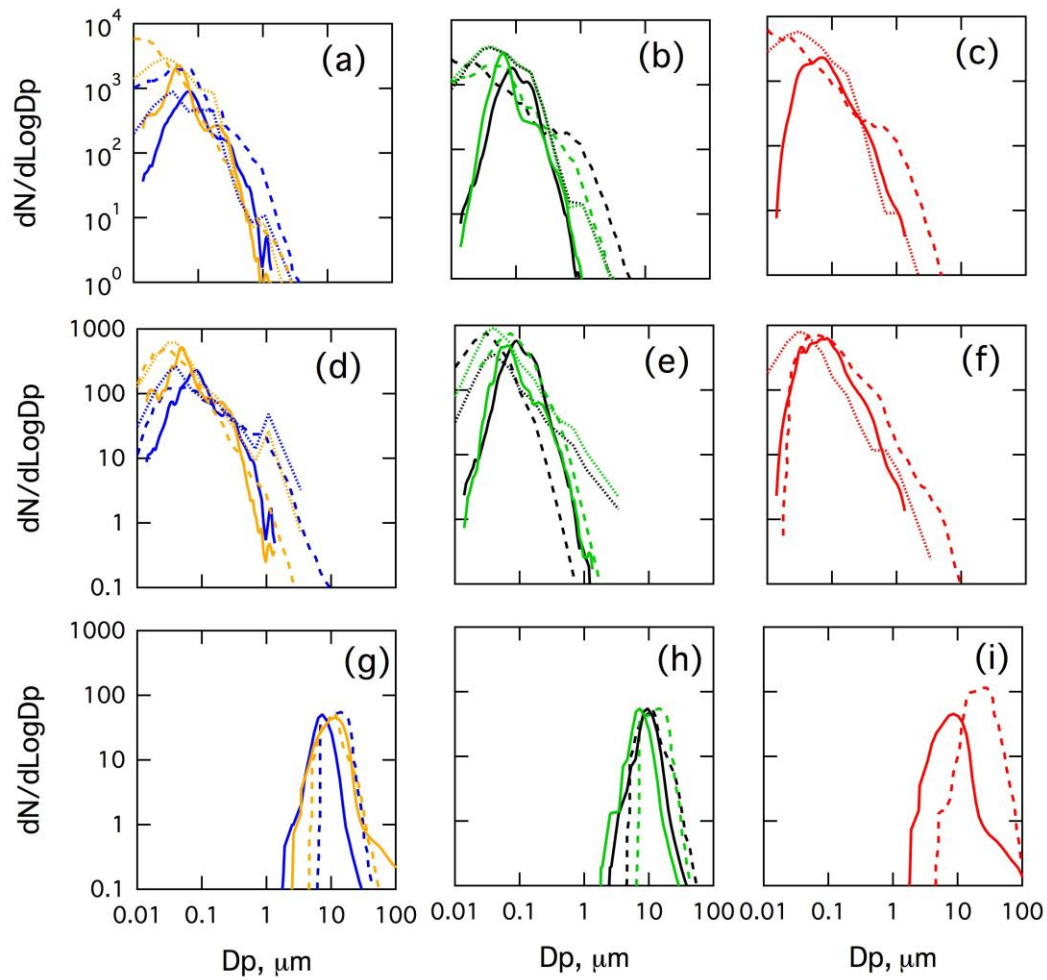


Figure 5.3: Comparison of the number size distribution of the (a-c) total particles, (d-f) BC type particles, and (g-i) Cloud droplets. Line colors indicate the sites: TH (blue), SA (orange), LB (black), LJ (green), and RV (red). Solid lines show results from the parcel model, dashed lines are from *Jacobson* [2010], and dotted lines are from *Chen et al.* [2010a].

Location	Total Aerosol N_a cm^{-3}			Cloud Droplets N_{bc} , cm^{-3}		
	Obs.	Jacobson [2010]	Chen et al. [2010a]	Obs.	Jacobson [2010]	Chen et al. [2010a]
TH	7287	8187	7740	160	197	184
RV	14321	15130	15900	301	389	349
LJ	10178	12031	11871	216	284	251
LB	11295	16500	13450	289	291	276
SA	9231	11070	10600	221	254	231

Table 5.3: Comparison of the total aerosol and cloud droplet number concentration for the baseline case studies at the five California field sites from observations (this study), and the *Jacobson* [2010] and *Chen et al.* [2010a] models.

A more direct comparison of differences in aerosols among the three models is obtained by comparing the total (summed up) aerosol and CDN concentrations. This comparison for the two GCM based studies and the detailed parcel model is illustrated in Figure 5.4. The primary trend that we observed is the direct correlation in the number concentrations for both total aerosol particles and total CDN concentrations of the three models, i.e. all three models predict a higher concentration in the more polluted cases. Relative to this study, both GCMs have a larger absolute concentration by between 20% and 25% as discussed in the previous section. Both GCMs also predict a larger total concentration for the CDNs by between 17% and 22%, with larger CDNs tracking tracks the higher absolute aerosol concentrations.

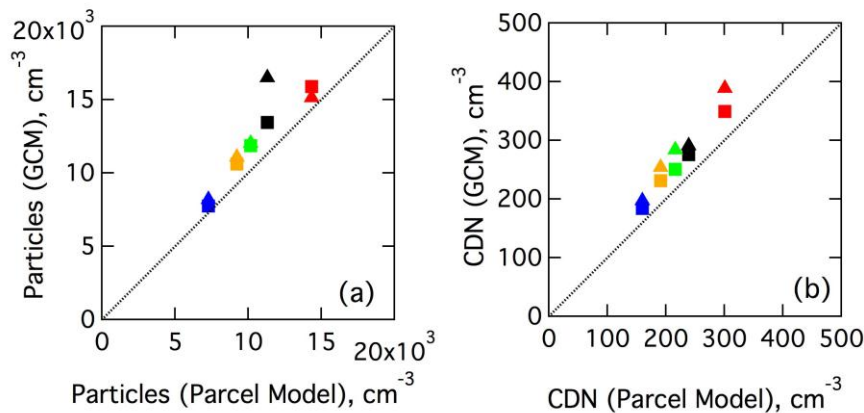


Figure 5.4: Comparison of (a) Total aerosol particle concentration and (b) CDN totals between the *Jacobson* [2010] (triangles) and *Chen et al.* [2010a] (squares) models compared to the field observations. Comparison is made at TH (blue), RV (red), LB (black), LJ (green), and SA (orange) sites.

5.7 Comparison of Mitigation Experiments

In addition to establishing correspondence among the three models at all five sites, our primary goal in this project is to examine and explain the differences in cloud droplets under BC mitigation scenarios. In order to constrain the BC effect, we compare our 50% BC mitigation scenario with the half-fossil fuel BC case from *Chen et al.* [2010a] and the no fossil soot (NFS) case from *Jacobson* [2010] (the latter being available only from the global run as a Northern Hemisphere average). The changes in total aerosol number concentration and CDN number are compared between the GCMs and the parcel model in Figure 5.5. We find that compared with the 7% to 11% decrease in particle number concentration from the parcel model, *Chen et al.* [2010a] find a larger decrease of between 18% and 20%. This larger reduction in particle number concentration by the *Chen et al.* [2010a] model is the result of their estimated decrease in the number concentrations of sulfate and organic particles from secondary particle formation associated with the reduced BC emissions (which are not identified by the ATOFMS characterization used in this study). *Jacobson* [2010] removed all fossil soot emissions and found a decrease slightly smaller than the observationally constrained particle concentrations in the parcel model of between 3% and 8%.

The change in CDN concentration for the reduced-BC cases largely tracked the reductions in BC aerosol concentration, with the *Chen et al.* [2010a] model finding the largest reduction, the *Jacobson* [2010] model finding the smallest magnitude change, and the chemically detailed, observationally-constrained parcel model in between. The parcel model found that the 50% BC case decreased CDN concentrations between 6% and 9%, which is comparable to the 9% to 12% decrease found by *Chen et al.* [2010a]. The larger decrease of *Chen et al.* [2010a] tracks the larger decrease in BC particle number concentration. On the other hand, *Jacobson* [2010], whose model included climate feedback and semi-direct effects, reported an increase in CDN concentration of 1% when fossil fuel emissions were eliminated. This increase was consistent for both the northern hemisphere and the global average in that study, but was not calculated for the nested-domain California studies discussed here.

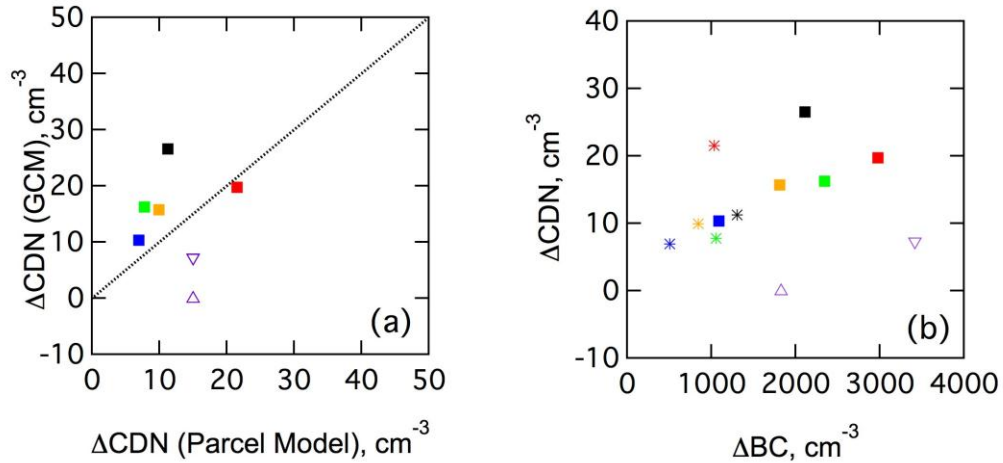


Figure 5.5: Comparison of (a) change in CDN number and (b) CDN number as a function of BC change between the *Jacobson [2010]* (triangles) and *Chen et al. [2010]* (squares) models compared to the field observations. Comparison is made at TH (blue), RV (red), LB (black), LJ (green), and SA (orange) sites.

To explain the differing responses to BC mitigation we propose the following explanation - BC particles in the *Chen et al. [2010a]* GCM and the parcel model are internally mixed with soluble species (such as organic acids, Ammonium Sulfate, and Ammonium Nitrate), making them somewhat hygroscopic. The *Jacobson [2010]* GCM treated fossil-fuel soot as evolving from externally-mixed to internally mixed. As a result, it was initially mostly hydrophobic but became more hygroscopic with aging. Biofuel soot, on the other hand, was more hygroscopic upon emissions because it was coated with more soluble chemicals and organic carbon. The no-fossil-soot case of that model then corresponds to the removal of particles that were not effective in acting as CDN, producing no significant corresponding reduction in the CDN concentration. A better comparison for California BC particles may be to the case that removes both fossil soot and biofuel burning soot, since the biofuel burning BC particles were modeled as more hygroscopic (which is consistent with the BC measured in California) and because the larger overall BC reduction represents a larger fraction of the average concentration (which is more similar to reducing only fossil fuel BC in California, since fossil fuel BC is a large fraction of the atmospheric concentration).

Location	Parcel Model (this work)		Jacobson [2010] model	Chen et al. [2010a] model
	50%BC	90%BC	NFS	HC
	% Change in total Aerosol Concentration			
TH	-6.9	-12.5	-2.3	-14.0
RV	-7.2	-13.1	-2.3	-18.1
LJ	-10.4	-18.6	-2.3	-19.7
LB	-11.5	-20.9	-2.3	-15.6
SA	-9.1	-16.4	-2.3	-17.1
	% Change in Cloud Droplet Concentration			
TH	-5.6	-11.5	+0.9	-5.6
RV	-5.6	-11.6	+0.9	-6.4
LJ	-6.5	-15.7	+0.9	-6.4
LB	-9.8	-17.1	+0.9	-9.6
SA	-8.4	-15.2	+0.9	-6.8

Table 5.4: Percent change in the total aerosol and cloud droplet number concentrations compared for the field studies under the 50% BC, 90% BC (this work), NFS (*Jacobson* [2010]), and HC (*Chen et al.* [2010a]) mitigation scenarios. The North Hemisphere average is used for the Jacobson model

It is important to note other possible explanations for the *Jacobson* [2010] model having a smaller change in CDN in the NFS case. This model included the semi-direct effect [*Hansen et al.*, 1997] and the cloud absorption effect [*Jacobson*, 2006] and precipitation changes, all of which can affect cloud droplet concentration. These climate feedback effects are not included in the *Chen et al.* [2010a] GCM or the parcel model calculations.

5.8 Conclusions

We have obtained aerosol particle size distributions and cloud droplet numbers corresponding to the California case studies from GCM simulations conducted by Professors Seinfeld and Jacobson, the latter of which was supported in part by collaborative funds from this project. We have compared the total aerosol number and cloud droplet number as determined from the cloud-aerosol parcel model based on field measurements with those predicted from GCMs for the base (total emissions) case, as well as the BC mitigated cases. We find that the total cloud droplet number agrees with the GCMs within 20%, which is acceptable given the variability between the three models. We have found that the reduction in cloud droplet number as predicted by the parcel model qualitatively agrees with the GCM of Professor Seinfeld, which does not include climate feedbacks. The reduction agrees with the GCM of Professor Jacobson only when the BC is treated as being hydrophilic. If BC is treated as being entirely hydrophobic, BC mitigation is found to increase the cloud droplet number due to climate feedbacks in conjunction with the low contribution of hydrophobic BC to cloud condensation nuclei number.

6.0 Sensitivity Studies and significance of results (Task 4)

6.1 Introduction

In addition to investigating the impact of BC mitigation for different aerosol mixings states in California (represented by the selected case studies), we have also completed a series of sensitivity studies to determine the impact of different model configurations. The completed sensitivity studies fall into three broad categories: 1) first, we have analyzed the effects of constraining the aerosol size and composition by varying the internal mixing state and size distribution of the aerosols, 2) second, we have analyzed the effect of different observed atmospheric conditions as represented in the parcel model by varying the surface temperature difference (in the variable updraft mode) and the updraft velocity (in the constant updraft mode) while keeping the aerosol concentration constant, and 3) finally we have compared the predicted cloud drop distributions to parameterizations that are currently implemented in GCM studies [Lohmann *et al.*, 2007] to establish if the cloud droplet number concentrations employed in GCMs are realistic for the measured aerosol concentrations in California.

6.2 Impact of Model Mechanisms

Figure 6.1 compares the CDN determined by applying the parcel model in conjunction with the marine stratocumulus cloud described in this work with the available GCM aerosol size distributions of *Chen et al.* [2010a] for both the base case and BC mitigation case and *Jacobson* [2010] for the base case (since detailed aerosol information for the mitigation case in California is not available). The different aerosol species (sulfate, EC, OC, and nitrate) were treated here as externally mixed. This comparison preserves the aerosol microphysical properties and therefore isolates the combined effect of the activation mechanisms and meteorology between the parcel model and the GCMs. In general, applying the parcel model produces CDNs that are between 2% (LB) and 16% (RV) higher than calculated by the GCMs for the base cases. For the corresponding BC reduction cases, the corresponding increase is between 2% (LB) and 11% (RV), indicating that the enhancement is higher for cases with a larger fraction of hygroscopic (non-BC) particles. Figure 6.1 (b) compares the fraction of total particles activated into cloud droplets for the corresponding cases. The trend is reproduced consistently, and a higher fraction of particles is seen to activate when the relative fraction of BC type particles is reduced.

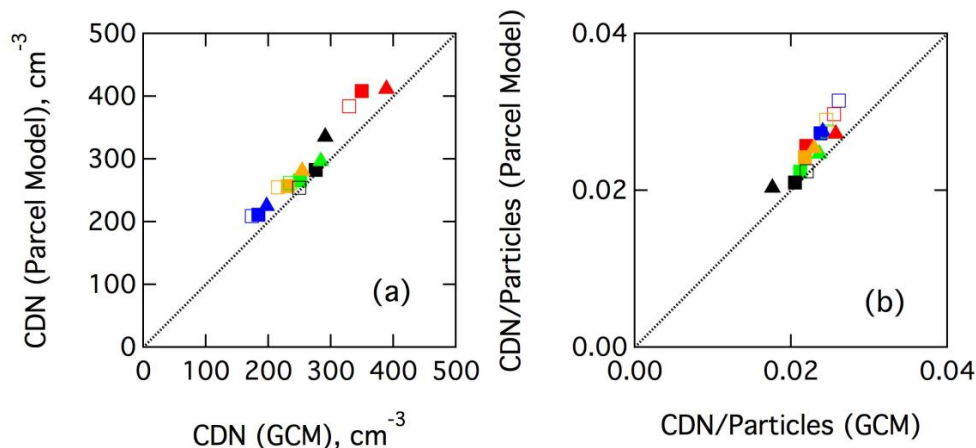


Figure 6.1. Comparison of the (a) total CDN and (b) CDN/Particle ratio determined from the GCMs by using a full climate simulation and by applying the parcel model and meteorology described in this work to the aerosol concentrations determined from the GCMs. The symbols used are the same as Figures 5.4 and 5.5.

6.3 Impact of Internal Mixing State

A central conclusion of this work is that hygroscopicity of BC (and all aerosol) particles may play a key role in determining their role as cloud nuclei. Since the internal mixing state described in Chapter 2 is not a uniquely measured composition, we examined the effect of varying the internal mixing states for the aerosol population types. We compared the total number of CDN activated under two conditions: first, determined by allowing internal mixing as described (maximum internal mixing), and second, by treating each species as being only externally mixed (no internal mixing). As an example in the second case, the nitrate type particles are only nitrate and the BC type particles are only BC. To constrain the no-internal mixing state scenarios to field measurements, we left the number size distributions for each particle type unchanged, conserving the total number of aerosol particles. This set of experiments aims to isolate the effect of chemical composition.

Particle Type	Nc with Internal Mixing, cm ⁻³	Nc with no Internal Mixing, cm ⁻³	% Change
BC	68±29	22±12	-67.6
OC	106±29	101±26	-4.7
Sulfate	35±5	37±6	+5.7
Nitrate	29±7	30±10	+3.4

Table 6.1: Average change in number of activated cloud droplets when aerosol particle types are treated as being internally mixed and as pure components.

The change in CDN concentrations is illustrated in Figure 6.2 for ten simulation cases. The number of activated sulfate and nitrate particles are found to increase

in each case, but typically by less than 5%. This is consistent with the bulk of these particles with internal mixing being composed of highly hygroscopic species that dominate the solution equilibrium. For the OC particle types, the number of activated particles is found to decrease by between 5% and 8%. This decrease is consistent with the reduction in hygroscopicity for this particle type when the sulfate and nitrate mass is replaced by OC. The biggest change is seen for the BC particle type, where the number of activating particles is reduced by between 70% and 80% compared to the case with internal mixing. Due to the relatively high supersaturation, some of the hydrophobic BC particles still activate, but this number is small compared to when some internal mixing with hygroscopic species is allowed. These trends support the result that the CDN change is more sensitive to change in BC concentration when the BC is at least partially hygroscopic.

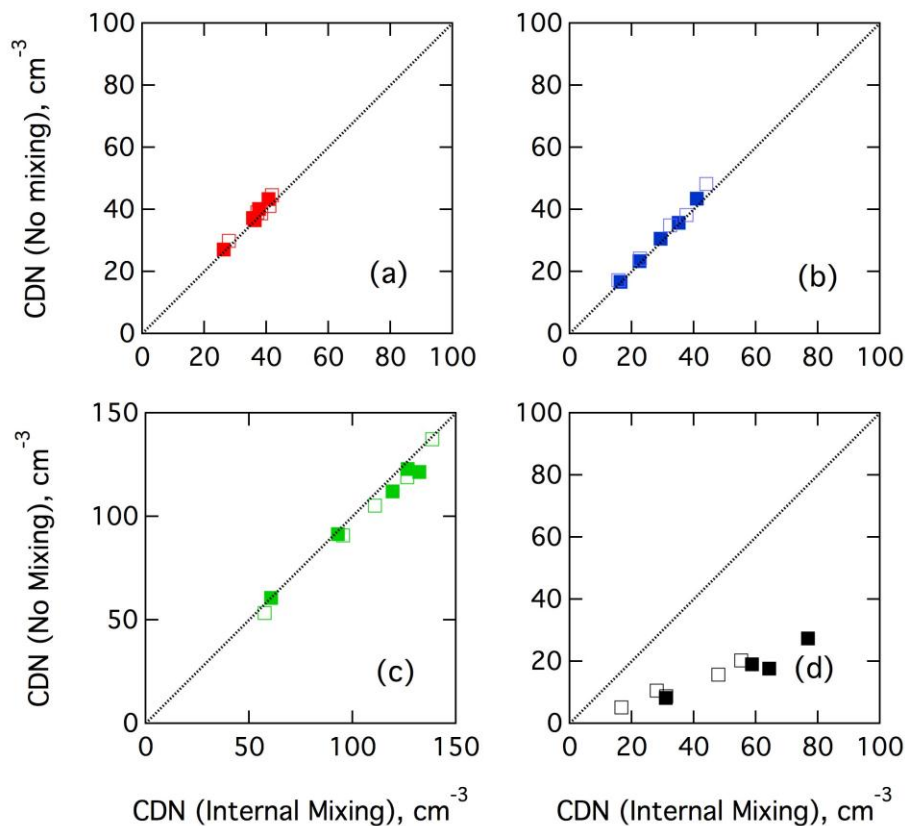


Figure 6.2. The total number of particles activated for (a) Sulfate, (b) Nitrate, (c) OC, and (d) EC type particles when no internal mixing is allowed, compared to the internal mixing states described in Chapter 2.

The Jacobson [2010] model provides two mitigation scenarios – the HF case more closely resembles the no-internal mixing case described here, where the BC is treated as originating from fresh fossil fuel emissions and is primarily composed of EC. In this case, we find BC particles act as very inefficient nuclei for clouds. The BC mitigation therefore does not reduce CDNs significantly (due

to the indirect effect), rather reduction in the semi-direct effects leads to the observed increase in cloud cover. The HFBFBG case, on the other hand, allows BC particles to contain hygroscopic OC from biogenic sources, more closely mirroring the full-internal mixing case from this study. Here, the BC particles are more efficient cloud nuclei and a decrease in BC particle number due to mitigation results in an observed decrease in the cloud droplet number.

6.4 Impact of Updraft Rate

The California scenarios for aerosol-cloud interactions described in Chapter 4 were completed using a simplified, yet relevant model for the ambient atmosphere based on measured temperature and humidity profiles. Since the droplet activation is determined kinetically in this work, the rate at which the aerosol parcel rises (or descends) through the cloud is a key parameter that can be used to describe different ambient conditions. As part of the refinements introduced to the model in this work, we calculated the parcel updraft velocity in two modes: (1) The fixed updraft mode with a constant updraft velocity for an observed range of values of 0.2 and 2.0 m s⁻¹ [Nicholls and Leighton, 1986] is used to establish representative values for maximum supersaturation, cloud droplet number concentration, and typical duration of a single cloud cycle, as in Russell et al. [2000]. In this mode, the slower updraft velocities represent calm conditions and the higher velocities represent more stormy conditions. The key assumption is that the aerosol parcel is subject to preselected meteorological conditions that do not vary over the course of the (relatively short) cloud cycle. (2) The calculated updraft mode initialized by a surface temperature difference of +1.0 K relative to the ambient at sea level [Lucas et al., 1994] is used to represent near-adiabatic cloud conditions. The calculated updraft mode follows the treatment of [Pruppacher and Klett, 2003] developed for convective clouds, calculating the updraft velocity at each time step while allowing the adiabatic cooling of the aerosol parcel and entrainment of humid air. This mode allows for an improved representation of ambient conditions since it includes effects due to the total aerosol concentration and chemistry, expressed indirectly as total latent heat and heat capacity of the parcel.

The impact of varying the updraft velocity in the constant updraft mode (and variations in the prescribed surface temperature difference and entrainment in the calculated updraft mode) on the maximum supersaturation and CDN concentration is illustrated in Figure 6.3. For the calculated updraft, both the updraft velocity at the point of maximum supersaturation and the mean updraft velocity up to that point are shown. Prescribing a surface temperature difference between 0.5 and 1.5K produces mean updraft velocities between 0.3 and 0.9 m s⁻¹ that are consistent with field measurements in clouds [Emanuel and Bister, 1996; Nicholls and Leighton, 1986]. Faster updrafts allow for a higher maximum supersaturation (0.3% and 0.5% respectively), and the trend is consistent with the constant updraft mode, where fixed updraft velocities between 0.2 and 1.6 m s⁻¹ produce maximum supersaturation varying between 0.3 and 1.0%. The CDN

concentration varies by a small amount between 312 cm^{-3} and 283 cm^{-3} over this range of velocities, indicating that activation determined kinetically by integrating the largest size mode is limited by the total amount of available water vapor and aerosol concentration rather than updraft conditions.

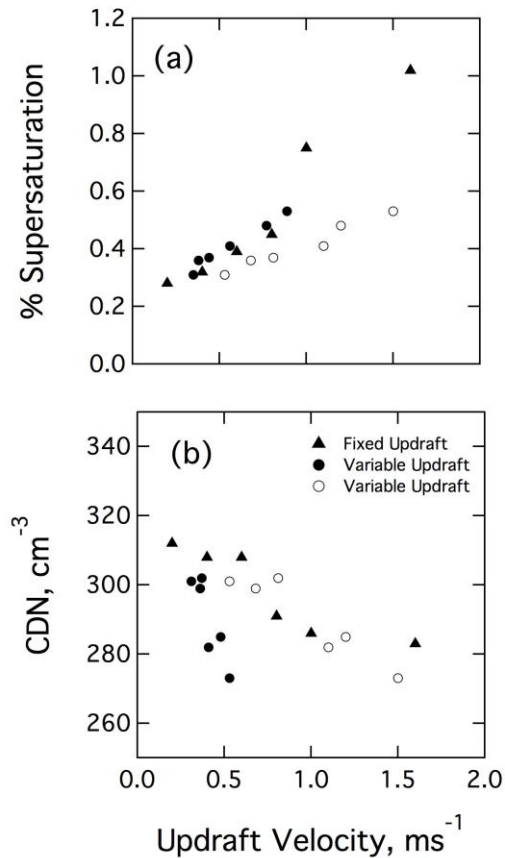


Figure 6.3: Parcel model simulations of the dependence on the updraft velocity operating in fixed updraft (triangles) and energy conservation (circles) mode: (a) maximum supersaturation and (b) cloud droplet number concentration. Empty circles indicate updraft at maximum supersaturation and filled circles indicate mean updraft velocity up to the maximum supersaturation.

6.5 Comparison with GCM Parameterization

The work undertaken in this study quantifies the first aerosol indirect effect by determining the variation in total cloud droplets as aerosol (specifically BC) concentrations are varied. To gain a better understanding of this as it relates to aerosol forcing, we compare the changes in CDN determined here with the parameterizations used in GCMs (that evaluate the aerosol forcing). There is no consensus on parameterizing cloud droplet concentrations in the GCM community, as a recent study [Ghan *et al.*, 2011] compared a number of complex cloud activation parameterizations and found significant differences in the maximum supersaturation and critical droplet diameters depending on the aerosol properties and updraft conditions. For this work, we have applied the

parameterization of [Nenes and Seinfeld, 2003] to the measured aerosol size distributions in California. We used the same temperature, pressure, and updraft conditions used to describe stratocumulus clouds in Chapters 3 and 4 for this series of experiments. Meteorological conditions at the cloud base are used to determine the maximum supersaturation and corresponding cloud droplet number in a series of simplified offline calculations.

Location	Parcel Model		Parameterization	
	N_c cm^{-3}	S_{max} %	N_c cm^{-3}	S_{max} %
TH	160	0.38	202	0.43
RV	301	0.24	338	0.27
LJ	216	0.27	243	0.31
LB	289	0.25	318	0.27
SA	221	0.34	257	0.37

Table 6.2: Comparison of cloud droplet number concentration and maximum supersaturation for the case studies obtained using the aerosol-cloud parcel model and the Nenes and Seinfeld [2003] parameterization.

The maximum supersaturation and CDN calculated using the parameterization are compared to the full parcel model results in Figure 6.4, and summarized in Table 6.2. For the California case studies, the parameterization calculations determine a slightly higher maximum supersaturation, which results in a slightly larger number of cloud droplets activating. There are a number of factors that contribute to this difference. First, slight differences in the value of thermodynamic variables such as the enthalpy of phase change of water, and thermal conductivity used in the model and parameterizations lead to slightly different equilibrium conditions. Second, the parameterization assumes a simplified shape of the Köhler curves and supersaturation to obtain a closed solution that leads to different growth rates compared to the parcel model that calculates time dependent and size resolved growth rates. Third, the parameterization uses the temperature, pressure, and vertical velocity at the cloud base to approximate their values at the maximum supersaturation level, but it does not take into account how these evolve as the parcel travels upward in the cloud. Finally, any droplet reduction through the “deactivation” mechanism of Nenes *et al.* [2001] above the point of maximum supersaturation is not accounted for by the parameterization and may (under conditions of very high CCN) lead to some over-prediction in droplet number compared to the parcel model. Overall however, the parameterizations and parcel model capture the droplet number well, and we believe that (in the context of climate models) we have successfully captured the first indirect effect and constrained it to measurements of aerosol distributions in California.

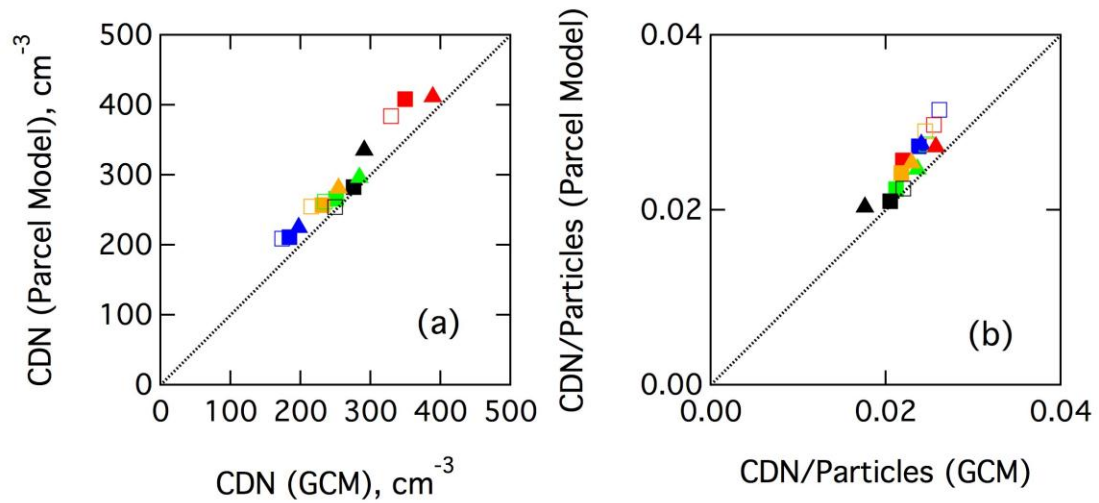


Figure 6.4. Comparison of the (a) total CDN and (b) CDN/Particle ratio determined from the GCMs using a full climate simulation, and by applying the parcel model and meteorology described in this work to the aerosol concentrations determined from the GCMs. The symbols used are the same as Figure 6.1.

7.0 Conclusions and Findings

7.1 Primary Conclusion

To better constrain the first aerosol indirect effect of BC, we have used a chemically-detailed microphysical parcel model to analyze measured baseline and BC mitigation scenarios in California. Aerosol particles were modeled as external mixtures of internally mixed chemical components based that are representative of different emissions in California. We have assessed one aspect of the aerosol indirect effect of BC mitigation by comparing the total CDN in the mitigation scenarios with GCM calculations based on emission inventories. We find that the particle number size distributions agree well for the three model types, though BC particles in the parcel model are smaller than the GCMs possibly because the locations and seasons of the field campaigns did not represent all of the particle sources included in the GCMs.

The central conclusion of this work can be summed up as follows: In the polluted California environment, BC-type particles contribute between 14% and 18% of the total cloud droplets. The parcel model predicted that BC mitigation reduces the droplet population in clouds by between 5% and 9% for 50% BC mitigation, and 11% and 17% for 90% BC mitigation. This result agrees well with predictions for the half fossil fuel case from the *Chen et al.* [2010a] model (with a smaller relative magnitude). The predicted decrease in CDN by these two models differs from the *Jacobson* [2010] model which found that fossil soot mitigation (in isolation from biomass burning soot) caused a 1% increase in CDN concentration. This difference was likely the result of that model's treatment of fossil fuel BC particles as initially hydrophobic, although its inclusion of semi-direct and cloud absorption feedbacks could have also reduced CDN by reducing cloud supersaturation. A complete understanding of the BC mitigation in California and the rest of the world (including processes such as the impact on sea ice and land glaciers) requires further work to better constrain the other effects of BC on climate.

7.2 Research Highlights

1. We have identified five field campaigns in California that represent a variety of ambient conditions with the most complete available chemical and physical measurements of externally mixed particles; the sites are: Clean Marine (Trinidad Head), Polluted Urban (Riverside and Sacramento), Polluted Marine (Long Beach), and Biomass Burning dominated (La Jolla).
2. For these case studies we have obtained ATOFMS measurements of the size resolved single particle measurements that provide the internal chemical mixing state of the different types of aerosol particles.
3. Based on chemical tracer analysis we have used these measurements to classify the aerosol particles as being EC dominated (from fossil fuel

- combustion), OC dominated (from secondary organic condensation and biomass burning), and Sulfate/Nitrate dominated (from SO₂/NO_x chemistry).
4. We have also obtained co-located SMPS and APS measurements of the number size distributions of the aerosol particles.
 5. We have obtained density measurements of the chemical particle types identified by the ATOFMS from literature based on laboratory studies.
 6. We have synthesized these three sets of measurements to describe the aerosol particles to initialize their physical (size and mass) and chemical (both internal and external mixing states) properties in the aerosol model for each site.
 7. We have set up a scenario describing idealized cloud-aerosol interactions in California by constructing temperature and humidity profiles that describe a continentally influenced marine stratus cloud.
 8. We have used our detailed parcel model in conjunction with the cloud profiles and observationally constrained aerosol populations to analyze the evolution of aerosol number size distributions at each of the case studies identified in Task 1.
 9. Based on the change in the aerosol number size distribution in the scenario runs, we have determined the total number of activated cloud droplets based on the growth of a mode at 10 μm.
 10. We have repeated the model analysis using scenarios constraining the EC dominated particle types to 50% and 90% of the measured population to determine the impact of BC mitigation on cloud droplet population.
 11. In addition to constraining the aerosol particle population, we have also completed a number of sensitivity studies by using the model to describe a variety of observed ambient conditions by altering the updraft velocity, allowing for adiabatic cooling, changing the air entrainment rate, and conserving the total available water vapor.
 12. We scheduled and organized an on-site meeting with Professor Seinfeld and Professor Jacobson. The meeting was also attended by CARB representatives, and Professor Ramanathan from SIO and Professor Prather from UCSD.
 13. We have obtained aerosol particle size distributions and cloud droplet numbers corresponding to the California case studies from GCM simulations conducted by Professors Seinfeld and Jacobson.
 14. We have compared the total aerosol number and cloud droplet number as determined from the cloud-aerosol parcel model based on field measurements with those predicted from GCMs for the base (total emissions) case, as well as the BC mitigated cases. We find that the total cloud droplet number agrees with the GCMs within a factor of 10-20%, which is acceptable given the variability between the three models. These results have been shared fully with Professor Mark Jacobson and Professor John Seinfeld
 15. We have found that the reduction in cloud droplet number as predicted by the parcel model qualitatively agrees with the GCM of Professor Seinfeld, which does not include climate feedbacks. The reduction agrees with the GCM of Professor Jacobson only when the BC is treated as being hydrophilic. If BC is

- treated as being entirely hydrophobic, BC mitigation is found to increase the cloud droplet number due to climate feedbacks in conjunction with poor contribution of hydrophobic BC to cloud condensation nuclei number.
16. The implications of this comparison are that in addition to the total BC and aerosol number concentration, the internal mixing state of the BC (which determines hygroscopicity) is also a significant factor in determining the net impact on clouds.
 17. We have completed our analysis of the impact of varying atmospheric conditions - represented in the parcel model by the total available water vapor, the surface temperature difference between the aerosol and ambient air, and the air entrainment rate, in both the energy conservation mode and the constant updraft mode. We find that the total activated cloud droplet number (CDN) depends primarily on the total aerosol concentration, and hygroscopicity of the aerosol (internal mixing state), with sulfate, nitrate, and OC containing particles activating at a significantly higher rate than EC containing particles – approximately 10% compared to 4% respectively.
 18. Repeating the BC mitigation experiments with the parcel model operating in constant updraft mode reproduced maximum supersaturation, and total cloud droplet number that were consistent with the energy conservation mode, supporting the robust nature of the results.
 19. A large range of aerosol concentrations (between 6000-14000 cm^{-3}) were analyzed using the parcel model over the course of this study, and they were found to produce an equivalent range of cloud droplets (between 151-300 cm^{-3}). These results indicate that the variability in calculated CDN between different case studies considered in California, as well as between the measured base case and BC mitigation cases are statistically significant and physically relevant for the conditions modeled.

References

- Adams, P. J., and J. H. Seinfeld (2002), Predicting global aerosol size distributions in general circulation models, *Journal of Geophysical Research-Atmospheres*, 107(D19), 23.
- Allen, J. O., et al. (2000), Particle detection efficiencies of aerosol time of flight mass spectrometers under ambient sampling conditions, *Environ Sci Technol*, 34(1), 211-217.
- Andreae, M. O., and P. Merlet (2001), Emission of trace gases and aerosols from biomass burning, *Global Biogeochemical Cycles*, 15(4), 955-966.
- Andreae, M. O., and D. Rosenfeld (2008), Aerosol-cloud-precipitation interactions. Part 1. The nature and sources of cloud-active aerosols, *Earth-Sci. Rev.*, 89(1-2), 13-41.
- Bahadur, R., et al. (2010), Composition and Morphology of Individual Combustion, Biomass Burning, and Secondary Organic Particle Types Obtained Using Urban and Coastal ATOFMS and STXM-NEXAFS Measurements, *Aerosol Science and Technology*, 44(7), 551-562.
- Bahadur, R., et al. (2011), Impact of California's air pollution laws on black carbon and their implications for direct radiative forcing, *Atmos Environ*, 45(5), 1162-1167.
- Bauer, S. E., et al. (2010), A global modeling study on carbonaceous aerosol microphysical characteristics and radiative effects, *Atmospheric Chemistry and Physics*, 10(15), 7439-7456.
- Bhave, P. V., et al. (2002), A field-based approach for determining ATOFMS instrument sensitivities to ammonium and nitrate, *Environ Sci Technol*, 36(22), 4868-4879.
- Bond, T. C., et al. (2004), A technology-based global inventory of black and organic carbon emissions from combustion, *Journal of Geophysical Research-Atmospheres*, 109(D14).
- Cantrell, W., et al. (1999), Cloud properties inferred from bimodal aerosol number distributions, *Journal of Geophysical Research-Atmospheres*, 104(D22), 27615-27624.
- Chen, W. T., et al. (2010a), Will black carbon mitigation dampen aerosol indirect forcing?, *Geophys Res Lett*, 37, 5.

- Chen, W. T., et al. (2010b), Global climate response to anthropogenic aerosol indirect effects: Present day and year 2100, *Journal of Geophysical Research-Atmospheres*, 115.
- Chung, S. H., and J. H. Seinfeld (2005), Climate response of direct radiative forcing of anthropogenic black carbon, *JGR*, 110(D11), doi: 000229829100007.
- Clarke, A. D., and K. J. Noone (1985), Soot in the Arctic Snowpack - a Cause for Perturbations in Radiative-Transfer, *Atmospheric Environment*, 19(12), 2045-2053.
- Clegg, S. L., et al. (1998), Thermodynamic model of the system $\text{H}^+ \text{-NH}_4^+ \text{-SO}_4^{2-} \text{-NO}_3^- \text{-H}_2\text{O}$ at tropospheric temperatures, *J Phys Chem A*, 102(12), 2137-2154.
- Durkee, P. A., et al. (2000), The Monterey Area Ship Track experiment, *Journal of the Atmospheric Sciences*, 57(16), 2523-2541.
- Dusek, U., et al. (2006), CCN Activation of Pure and Coated Carbon Black Particles, *Environmental Science & Technology*, 40(4), 1223-1230.
- Emanuel, K. A., and M. Bister (1996), Moist convective velocity and buoyancy scales, *Journal of the Atmospheric Sciences*, 53(22), 3276-3285.
- Erlick, C., et al. (2001), A microphysics-based investigation of the radiative effects of aerosol-cloud interactions for two MAST Experiment case studies, *Journal of Geophysical Research-Atmospheres*, 106(D1), 1249-1269.
- Forster, P., et al. (2007), Changes in Atmospheric Constituents and in Radiative Forcing, in *Climate Change 2007 : The physical Science Basis. Contribution of Working Group I to the Fourth Assessment Report of the Intergovernmental Panel on Climate Change*, edited by S. Solomon, et al., Cambridge University Press, Cambridge, UK and New York, USA.
- Fountoukis, C., and A. Nenes (2005), Continued development of a cloud droplet formation parameterization for global climate models, *Journal of Geophysical Research-Atmospheres*, 110(D11).
- Ghan, S. J., et al. (2011), Droplet Nucleation: Physically-based parameterizations and comparative evaluation, *Journal of Advances in Modeling Earth Systems*, 3, M10001.
- Guibert, S., et al. (2003), Aerosol activation in marine stratocumulus clouds: 1. Measurement validation for a closure study, *Journal of Geophysical Research-Atmospheres*, 108(D15), 17.

- Hansen, J., et al. (1997), The missing climate forcing, *Philos. Trans. R. Soc. B-Biol. Sci.*, 352(1350), 231-240.
- Hansen, J., and L. Nazarenko (2004), Soot climate forcing via snow and ice albedos, *Proceedings of the National Academy of Sciences of the United States of America*, 101(2), 423-428.
- Jacobson, M. Z. (2001), Control of black carbon, the most effective means of slowing global warming, *Computational Science -- Iccs 2001, Proceedings Pt 2, 2074*, 1060-1060.
- Jacobson, M. Z. (2002), Control of fossil-fuel particulate black carbon and organic matter, possibly the most effective method of slowing global warming, *Journal of Geophysical Research-Atmospheres*, 107(D19), 22.
- Jacobson, M. Z. (2006), Effects of externally-through-internally-mixed soot inclusions within clouds and precipitation on global climate, *Journal of Physical Chemistry A*, 110(21), 6860-6873.
- Jacobson, M. Z. (2010), Short-term effects of Controlling Fossil-Fuel Soot, Biofuel Soot and Gases, and Methane on Climate , Arctic Ice, and Air Pollution Health, *Journal of Geophysical Research-Atmospheres*, 115(D14).
- Koch, D., et al. (2009), Distinguishing Aerosol Impacts on Climate over the Past Century, *Journal of Climate*, 22(10), 2659-2677.
- Koch, D., and A. D. Del Genio (2010), Black carbon semi-direct effects on cloud cover: review and synthesis, *Atmospheric Chemistry and Physics*, 10(16), 7685-7696.
- Koch, D., et al. (2011), Soot microphysical effects on liquid clouds, a multi-model investigation, *Atmospheric Chemistry and Physics*, 11(3), 1051-1064.
- Koehler, K. A., et al. (2009), Cloud condensation nuclei and ice nucleation activity of hydrophobic and hydrophilic soot particles, *Phys. Chem. Chem. Phys.*, 11(36), 7906-7920.
- Kristjansson, J. E., et al. (2005), Response of the climate system to aerosol direct and indirect forcing: Role of cloud feedbacks, *Journal of Geophysical Research-Atmospheres*, 110(D24).
- Lammel, G., and T. Novakov (1995), Water nucleation properties of carbon black and diesel soot particles, *Atmospheric Environment*, 29(7), 813-823.
- Lim, H. J., et al. (2003), Semicontinuous aerosol carbon measurements: Comparison of Atlanta Supersite measurements, *Journal of Geophysical Research-Atmospheres*, 108(D7), -.

- Lohmann, U., and J. Feichter (2005), Global indirect aerosol effects: a review, *Atmospheric Chemistry and Physics*, 5, 715-737.
- Lu, M. L., et al. (2007), The Marine Stratus/Stratocumulus Experiment (MASE): Aerosol-cloud relationships in marine stratocumulus, *J Geophys Res-Atmos*, 112(D10).
- Lucas, C., et al. (1994), Convective Available Potential-Energy in the Environment of Oceanic and Continental Clouds - Correction and Comments, *Journal of the Atmospheric Sciences*, 51(24), 3829-3830.
- Meskhidze, N., et al. (2005), Evaluation of a new cloud droplet activation parameterization with in situ data from CRYSTAL-FACE and CSTRIFE, *J Geophys Res-Atmos*, 110(D16).
- Moffet, R. C., et al. (2008), Measurement of ambient aerosols in northern Mexico City by single particle mass spectrometry, *Atmospheric Chemistry and Physics*, 8(16), 4499-4516.
- Nenes, A., et al. (2001), Kinetic limitations on cloud droplet formation and impact on cloud albedo, *Tellus Series B-Chemical and Physical Meteorology*, 53(2), 133-149.
- Nenes, A., and J. H. Seinfeld (2003), Parameterization of cloud droplet formation in global climate models, *Journal of Geophysical Research*, 108(D14), 4415.
- Nicholls, S., and J. Leighton (1986), An Observational Study of the Structure of Stratiform Cloud Sheets .1. Structure, *Quarterly Journal of the Royal Meteorological Society*, 112(472), 431-460.
- Ogren, J. A., and R. J. Charlson (1983), Elemental Carbon in the Atmosphere - Cycle and Lifetime, *Tellus Series B-Chemical and Physical Meteorology*, 35(4), 241-254.
- Penner, J. E., et al. (1994), Quantifying and Minimizing Uncertainty of Climate Forcing by Anthropogenic Aerosols, *Bulletin of the American Meteorological Society*, 75(3), 375-400.
- Popovicheva, O., et al. (2008), Water interaction with hydrophobic and hydrophilic soot particles, *Physical Chemistry Chemical Physics*, 10(17), 2332-2344.
- Pratt, K. A., et al. (2010), In Situ Chemical Characterization of Aged Biomass-Burning Aerosols Impacting Cold Wave Clouds, *Journal of the Atmospheric Sciences*, 67(8), 2451-2468.
- Pruppacher, H. R., and J. D. Klett (2003), *Microphysics of Clouds and Precipitation*, Kluwer Academic, Norwell, MA.

- Qin, X. Y., et al. (2006), Comparison of two methods for obtaining quantitative mass concentrations from aerosol time-of-flight mass spectrometry measurements, *Analytical Chemistry*, 78(17), 6169-6178.
- Ramanathan, V., et al. (2007), Warming trends in Asia amplified by brown cloud solar absorption, *Nature*, 448, 575-578.
- Roberts, G., et al. (2003a), Impact of biomass burning on cloud properties in the Amazon Basin, *J Geophys Res*, 108, doi: 10.1029/2001/JD000985.
- Roberts, G. C., et al. (2003b), Impact of biomass burning on cloud properties in the Amazon Basin, *Journal of Geophysical Research-Atmospheres*, 108(D2).
- Russell, L. M., and J. H. Seinfeld (1998), Size- and composition-resolved externally mixed aerosol model, *Aerosol Science and Technology*, 28(5), 403-416.
- Russell, L. M., et al. (1999), Aerosol dynamics in ship tracks, *Journal of Geophysical Research-Atmospheres*, 104(D24), 31077-31095.
- Russell, L. M., et al. (2011), Identifying organic aerosol sources by comparing functional group composition in chamber and atmospheric particles, *Proc. Natl. Acad. Sci. U. S. A.*, 108(9), 3516-3521.
- Silva, P. J., and K. A. Prather (1997), On-line characterization of individual particles from automobile emissions, *Environmental Science & Technology*, 31(11), 3074-3080.
- Silva, P. J., et al. (1999), Size and chemical characterization of individual particles resulting from biomass burning of local Southern California species, *Environmental Science & Technology*, 33(18), 3068-3076.
- Snider, J. R., et al. (2003), Aerosol activation in marine stratocumulus clouds: 2. Kohler and parcel theory closure studies, *Journal of Geophysical Research-Atmospheres*, 108(D15), 23.
- Sodeman, D. A., et al. (2005), Determination of single particle mass spectral signatures from light-duty vehicle emissions, *Environ Sci Technol*, 39(12), 4569-4580.
- Spracklen, D. V., et al. (2011), Global cloud condensation nuclei influenced by carbonaceous combustion aerosol, *Atmospheric Chemistry and Physics*, 11(17), 9067-9087.
- Stier, P., et al. (2007), Aerosol absorption and radiative forcing, *Atmospheric Chemistry and Physics*, 7(19), 5237-5261.

- Suess, D. T., and K. A. Prather (1999), Mass spectrometry of aerosols, *Chemical Reviews*, 99(10), 3007.
- Ten Hoeve, J.E et al. (2012) Comparing results from a physical model with satellite and in situ observations to determine whether biomass burning aerosols over the Amazon brighten or burn off clouds, *Journal of Geophysical Research-Atmospheres*, 117, D08203, doi:10.1029/2011JD016856.
- Svenningsson, B., et al. (2006), Hygroscopic growth and critical supersaturations for mixed aerosol particles of inorganic and organic compounds of atmospheric relevance, *Atmos Chem Phys*, 6, 1937-1952.
- Zuberi, B., et al. (2005), Hydrophilic properties of aged soot, *Geophysical Research Letters*, 32(1).